Journal of Scientific Computing (2020) 83:50
https://doi.org/10.1007/s10915-020-01229-6

Structure-Preserving Numerical Approximations to a Non-isothermal Hydrodynamic Model of Binary Fluid Flows

Shouwen Sun[1] · Jun Li[2] · Jia Zhao[3] · Qi Wang[4]

Received: 21 November 2019 / Revised: 5 April 2020 / Accepted: 4 May 2020 / Published online: 3 June 2020

Abstract
We present two second order, structure-preserving numerical schemes for a newly derived thermodynamically consistent, non-isothermal hydrodynamical phase field model for incompressible binary viscous fluid flows. The schemes preserve the volume of each fluid phase, the total energy and the positive entropy production rate. The entropy quadratization approach is employed to devise the two semi-discrete numerical schemes in time, preserving both the total energy and the positive entropy production rate. The first scheme is weakly nonlinear, which is solved using iterative methods aided by fast Fourier algorithms. The second scheme is linear, in which a time-dependent supplementary variable is added to preserve the positive entropy production rate. The semi-discrete schemes are discretized in space by a finite difference method on staggered grids subsequently to yield two fully discrete schemes. Mesh refinement is carried out to confirm the order of the schemes and several numerical examples are provided to show hydrodynamic as well as thermal effects in resolving thermocapillary convection near the fluid interface in the incompressible binary viscous fluid flow.

Keywords Thermodynamical consistency · Nonisothermal binary incompressible viscous fluid flows · Entropy quadratization · Structure-preserving · Phase field · Supplementary variable method

✉ Qi Wang
qwang@math.sc.edu

Shouwen Sun
sunshouwen@csrc.ac.cn

Jun Li
nkjunli@foxmail.com

Jia Zhao
jia.zhao@usu.edu

[1] Beijing Computational Science Research Center, Beijing 100193, China

[2] School of Mathematical Sciences, Tianjin Normal University, Tianjin 300387, China

[3] Department of Mathematics & Statistics, Utah State University, Logan, UT 84322, USA

[4] Department of Mathematics, University of South Carolina, Columbia, SC 29208, USA

1 Introduction

Multiphase fluid flows are abundant in nature as well as in industrial settings. One of the useful methods of describing hydrodynamics of multi-phase fluid flows is the phase field method, which has emerged as an important modeling and computational tool in recent years [4,5,7,8,14,22,26,30,32,33]. The set of governing equations in phase field models for multiphase fluid flows is often derived variationally from its free energy functional guided by the generalized Onsager principle or equivalently the second law of thermodynamics [28]. There are a large number of works available for isothermal multiphase fluid flows, in which the most widely studied phase field model for binary fluid flows is the one for fluid mixtures of two incompressible viscous fluids of identical densities [15,18]. For phase field models, the energy quadratization (EQ) method and its variant scalar auxiliary variable (SAV) method have simplified the development of energy stable schemes significantly and make their development systematically [29,31,34].

In reality, non-isothermal settings are the norm in contrast to the idealization of the isothermal environment. To describe a fluid system faithfully, nonisothermal model must be employed. Recently, Guo and Lin presented a thermodynamically consistent phase-field model for non-isothermal, two-phase incompressible viscous fluid flows using the second law of thermodynamics [12]; Liu et al. proposed a general framework to derive transport equations with heat flows through the energetic variational approach [20]. They also derived a model describing the evolution of a nematic liquid crystal material subject to thermal effects [9]. In addition, since Benard's experimental study of convective pattern in a thin liquid layer heated from below, the type of "cellular" motion has been extensively studied theoretically and experimentally [2,23,24,35]. In many engineering applications, people are interested in understanding convective flow behavior in nonisothermal, multilayer/multiphase fluid systems, which are associated with two well-known instabilities, the Rayleigh–Benard instability and the Gibbs–Marangoni effect, both of which can lead to roll cell convection in the fluid. The instabilities are also referred to as the Rayleigh–Benard convection and the Benard–Marangoni convection or the thermocapillary convection, respectively. Buoyancy resulting from thermally induced density gradients under the influence of gravity leads to the Rayleigh–Benard convection; while interfacial forces due to surface tension variations produced by temperature or concentration gradients causes the Marangoni effect[25].

The characteristics of the thermocapillary convection in two-layer, liquid–liquid systems are generally more complex due to the hydrodynamics and thermal interaction between fluid motions in the two adjacent liquid layers. There are two typical modes of the thermocapillary convection driven by surface tension: in one the external temperature difference is perpendicular to the fluid interface and, in the other, the external temperature gradient is parallel to the interface. For nonisothermal multiphase fluids, interfacial tension is affected by the temperature gradient across the material's interface. When the interface separating two fluids is exposed to a temperature gradient, the variation of temperature-dependent surface tension along with the fluid viscosity would induce shear stresses in the neighborhood of the fluid interface, which then induces a motion of the fluids in the neighborhood of the interface. This effect plays an important role in various industrial applications [12]. Likewise, under the influence of gravity, buoyancy convection due to the lift force plays a leading role in various industrial applications as well.

Given their prominent role in engineering applications, fluid convection under non-isothermal conditions has been one of the central themes in fluid dynamics and heat transfer. Liu and Valocchi put forward a phase-field-based hybrid model that combines the lattice

Boltzmann method with the finite difference method to simulate immiscible thermocapillary flows [19]. Liu and Roux [21] conducted a numerical study of flow characteristics of thermocapillary convection in a system composed of two immiscible liquid layers subject to a temperature gradient along their interfaces. In [12], Guo and Lin presented a thermodynamically consistent phase-field model for nonisothermal two-phase flows; in another paper [13], they used a phase field model to study Benard–Marangoni convection in a two-layer fluid system and showed that the underlying energy dissipation law in the isothermal case could be maintained. However, there have not been any references about structure-preserving numerical methods for truly non-isothermal cases.

The numerical method that can preserve some physical/structural properties of the model is called a structure-preserving numerical method [10]. In recent years, there has been a surge in the development of numerical methods for continuous dynamical systems to preserve certain invariant quantities of the continuous systems. For instance, a series of works have been published on energy stable methods to preserve the energy dissipation property or the rate of energy dissipation for multiphase fluid flows. Gong et al. [11] introduced an energy stable method for solving hydrodynamic phase field models of binary viscous fluids; Li et al. [17] presented a numerical scheme that preserves the total energy and the entropy production rate, termed the energy and entropy production rate preserving scheme, for a general class of thermodynamically consistent phase field models for dendritic crystal growth derived from the first and second law of thermodynamics. However, we have yet seen any structure-preserving numerical algorithms developed for thermodynamically consistent nonisothermal hydrodynamical models for multiphase fluid flows.

In this paper, we first extend the thermodynamically consistent phase field model for an isothermal, incompressible binary material system to nonisothermal, incompressible binary viscous fluid flows, taking into account the hydrodynamic effects and the thermal-hydrodynamic coupling. This hydrodynamic model is new in that it allows one to employ more accurate approximations for the internal energy as a function of the absolute temperature and phase variable as well as the latent heat. Using the entropy quadratization (EQ) approach coupled with a finite difference method on spatially staggered-grids, we propose and analyze a pair of second order schemes for the nonisothermal hydrodynamic phase field model consisting of the phase transport Cahn–Hilliard equation, Navier–Stokes equation with the extra stress and energy conservation equation derived from a non-equilibrium thermodynamic framework. In these two schemes, we use different mechanisms to preserve the positive entropy-production-rate and total energy at the discrete level.

The first structure-preserving scheme is weakly nonlinear in that the momentum balance couples with the energy balance equation nonlinearly in the scheme. We refer to it as the EQ scheme in this paper. In order to preserve the entropy-production-rate using the EQ approach, we have to settle with a weakly nonlinear scheme. In its numerical implementation, we employ iterative methods coupled with fast Fourier Transform algorithms to accelerate the computation [10]. The second structure-preserving scheme is linear known as the SVM scheme. This scheme is devised based on the entropy-quadratization approach as well as a new supplementary variable method (SVM). The supplementary variable method is a new framework for developing structure-preserving algorithms. The idea is to introduce a supplementary variable to the thermodynamically consistent model to enforce the entropy-production-rate after discretization. When this idea is coupled with the EQ strategy, the supplementary variable at each time marching step can be represented as a root of a quadratic equation. Therefore, the added computational cost is negligible. Theoretically, we show that the supplementary variable is of $O(\Delta t^2)$ where Δt is the time step size, retaining the order of the schemes at the second order. This is adequately confirmed in our numerical simulations.

Through conducting mesh refine tests on the two schemes, we confirm their rates of convergence. Then, we simulate the thermocapillarity effect in a two-layer incompressible viscous fluid system in an adiabatic (insulated) container, where the binary immiscible fluid system is confined in a bounded domain and subjected to an initial temperature gradient consistent with adiabatic boundary conditions.

The rest of the paper is organized as follows. In Sect. 2, we present the derivation of the hydrodynamic phase field model for a nonisothermal incompressible binary viscous fluid flows, and prove that the equation system is thermodynamically consistent. In Sect. 3, we introduce some notations, lemmas and definitions of grid functions in two-dimensional space. In Sect. 4, the entropy quadratization approach as well as the supplementary variable method are employed to derive semi-discrete numerical schemes in time, and the spatial discretization is carried out on the semi-discrete schemes using a finite difference method on staggered grids subsequently to yield the fully discrete schemes. We then prove that the fully discrete numerical schemes preserve both the energy balance, the volume of each fluid phase and the positive entropy-production-rate. In Sect. 5, we present numerical convergence tests to demonstrate the accuracy of the schemes and simulate thermocapillary convection in a two-layer, incompressible, viscous fluid system to show the usefulness of the schemes in resolving thermocapillary effect and retaining conservation of the fluid volume, energy balance and the positive entropy-production-rate. Finally, a concluding remark is given in Sect. 6.

2 Mathematical Formulation of the Nonisothermal Hydrodynamic Model of Incompressible Binary Viscous Fluid Flows

We develop a thermodynamically consistent hydrodynamic phase field model for an incompressible binary viscous fluid flows in the form of a Cahn–Hilliard equation coupled with the Navier–Stokes equation as well as the energy conservation equation. We call it the nonisothermal Cahn–Hilliard–Navier–Stokes equation system.

2.1 Conservation Laws

We assume that the binary fluid mixture is composed of two incompressible fluid components A and B, with ϕ representing the volume fraction of component A, $1-\phi$ the volume fraction of component B. $\rho_1 = \hat{\rho}_1\phi$, $\rho_2 = \hat{\rho}_2(1-\phi)$ are their respective densities, where $\hat{\rho}_1$ and $\hat{\rho}_2$ are the specific densities of the two fluid components, respectively. $\rho = \rho_1+\rho_2 = \hat{\rho}_1\phi+\hat{\rho}_2(1-\phi)$ is the mass density of the fluid mixture. We denote $\mathbf{v}$ the mass average velocity of the fluid mixture, T the absolute temperature, e the internal energy per unit volume and s the entropy per unit volume. In this paper, we consider the case where $\hat{\rho}_1 = \hat{\rho}_2$, i.e., the two constituents are of equal mass densities. So, $\rho = \hat{\rho}_1$ is a constant.

For a given material volume Ω, the total entropy S of the system is given by

$$S(e,\phi,\nabla\phi) = \int_\Omega s(e,\phi,\nabla\phi)d\mathbf{x} = \int_\Omega [s_0(e,\phi) + s_1(\nabla\phi)]d\mathbf{x}, \tag{2.1}$$

where $s_0(e,\phi)$ is the bulk part of the entropy and $s_1(\nabla\phi)$ is the conformational entropy. From mass conservation equation

$$\rho_t + \nabla \cdot (\rho \mathbf{v}) = 0, \tag{2.2}$$

we deduce

$$\nabla \cdot \mathbf{v} = 0. \tag{2.3}$$

The momentum conservation law states that

$$\rho \mathbf{v}_t + \rho \nabla \cdot (\mathbf{v}\mathbf{v}) = \nabla \cdot (\sigma_e + 2\eta \mathbf{D} - p\mathbf{I}) + \mathbf{b}, \tag{2.4}$$

where σ_e is the second order Ericksen stress tensor and σ_e is the term to be determined. $\mathbf{I}$ is the identity matrix, p is the hydrostatic pressure, η is the viscosity of the fluid, $D = \frac{1}{2}(\nabla \mathbf{v} + \nabla \mathbf{v}^T)$ is the rate of strain tensor, $\mathbf{b}$ is the external force density per unit volume (for example the gravity).

The energy conservation equation [3] is given by

$$\left(\frac{\rho}{2}|\mathbf{v}|^2 + e\right)_t + \nabla \cdot \left[\left(\frac{\rho}{2}|\mathbf{v}|^2 + e\right)\mathbf{v}\right] = \nabla \cdot [(\sigma_e + 2\eta \mathbf{D} - p\mathbf{I}) \cdot \mathbf{v}] - \nabla \cdot \mathbf{q} + \mathbf{b} \cdot \mathbf{v}, \tag{2.5}$$

where $\mathbf{q}$ is the heat flux. Taking the inner product of (2.4) with $\mathbf{v}$, we obtain

$$\left(\frac{\rho}{2}|\mathbf{v}|^2\right)_t + \nabla \cdot \left[\left(\frac{\rho}{2}|\mathbf{v}|^2\right)\mathbf{v}\right] = -(\sigma_e + 2\eta \mathbf{D}) : \nabla \mathbf{v} + \nabla \cdot [(\sigma_e + 2\eta \mathbf{D} - p\mathbf{I}) \cdot \mathbf{v}] + \mathbf{v} \cdot \mathbf{b}, \tag{2.6}$$

where $\mathbf{I} : \nabla \mathbf{v} = \nabla \cdot \mathbf{v} = 0$ is used. This gives the transport equation for the kinetic energy. Subtracting (2.6) from (2.5), the internal energy satisfies the following transport equation

$$e_t + \nabla \cdot (e\mathbf{v}) = (\sigma_e + 2\eta \mathbf{D}) : \nabla \mathbf{v} - \nabla \cdot \mathbf{q}. \tag{2.7}$$

Meanwhile, the equation for the volume fraction is proposed as follows:

$$\phi_t + \nabla \cdot (\phi \mathbf{v}) = j, \tag{2.8}$$

where $j = -\nabla \cdot J$ is the term to be determined and J is the excessive diffusive flux.

2.2 Second Law of Thermodynamics and the Onsager Principle

Next, we examine the entropy production rate of the system. Notice that $\frac{\delta S}{\delta e} = \frac{\partial s_0}{\partial e} = \frac{1}{T}$, so

$$\nabla s = \frac{\delta S}{\delta e}\nabla e + \frac{\delta S}{\delta \phi}\nabla \phi + \nabla \cdot \left(\frac{\partial s}{\partial \nabla \phi}\nabla \phi\right). \tag{2.9}$$

Then

$$\begin{aligned} -\left(\frac{\delta S}{\delta e}\nabla e + \frac{\delta S}{\delta \phi}\nabla \phi\right) \cdot \mathbf{v} &= -\left[\nabla s - \nabla \cdot \left(\frac{\partial s}{\partial \nabla \phi}\nabla \phi\right)\right] \cdot \mathbf{v} \\ &= \left(s\mathbf{I} - \frac{\partial s}{\partial \nabla \phi}\nabla \phi\right) : \nabla \mathbf{v} - \nabla \cdot \left[\left(s\mathbf{I} - \frac{\partial s}{\partial \nabla \phi}\nabla \phi\right) \cdot \mathbf{v}\right] \\ &= \left(-\frac{\partial s}{\partial \nabla \phi}\nabla \phi\right) : \nabla \mathbf{v} - \nabla \cdot \left[\left(s\mathbf{I} - \frac{\partial s}{\partial \nabla \phi}\nabla \phi\right) \cdot \mathbf{v}\right], \end{aligned} \tag{2.10}$$

where incompressibility condition (2.3) is used. The rate of entropy production is calculated as follows.

$$\frac{dS}{dt} = \int_\Omega \left(\frac{\delta S}{\delta e}e_t + \frac{\delta S}{\delta \phi}\phi_t\right) d\mathbf{x} + \int_{\partial\Omega} \mathbf{n} \cdot \left(\frac{\partial s}{\partial \nabla \phi}\phi_t\right) d\mathbf{a}$$

$$
\begin{aligned}
&= \int_\Omega \frac{\delta S}{\delta e}[-\nabla\cdot(e\mathbf{v}) + (\sigma_e + 2\eta\mathbf{D}) : \nabla\mathbf{v} - \nabla\cdot\mathbf{q}] \\
&\quad + \frac{\delta S}{\delta \phi}[-\nabla\cdot(\phi\mathbf{v}) - \nabla\cdot J]d\mathbf{x} + \int_{\partial\Omega} \mathbf{n}\cdot\left(\frac{\partial s}{\partial\nabla\phi}\phi_t\right)d\mathbf{a} \\
&= \int_\Omega \left[-\left(\frac{\delta S}{\delta e}e + \frac{\delta S}{\delta\phi}\phi\right)\mathbf{I} : \nabla\mathbf{v} - \left(\frac{\delta S}{\delta e}\nabla e + \frac{\delta S}{\delta\phi}\nabla\phi\right)\cdot\mathbf{v} + \frac{1}{T}(\sigma_e + 2\eta\mathbf{D}) : \nabla\mathbf{v}\right. \\
&\quad + \mathbf{q}\cdot\nabla\left(\frac{1}{T}\right) \\
&\quad \left. + \nabla\frac{\delta S}{\delta\phi}\cdot J\right]d\mathbf{x} + \int_{\partial\Omega}\mathbf{n}\cdot\left(\frac{\partial s}{\partial\nabla\phi}\phi_t - \frac{\mathbf{q}}{T} - \frac{\delta S}{\delta\phi}J\right)d\mathbf{a} \\
&= \int_\Omega \left[\frac{\delta S}{\delta e}\left(\sigma_e + 2\eta\mathbf{D} - T\frac{\partial s}{\partial\nabla\phi}\nabla\phi\right) : \nabla\mathbf{v} + \mathbf{q}\cdot\nabla\left(\frac{1}{T}\right) + \nabla\frac{\delta S}{\delta\phi}\cdot J\right]d\mathbf{x} \\
&\quad + \int_{\partial\Omega}\mathbf{n}\cdot\left[\frac{\partial s}{\partial\nabla\phi}\phi_t - \left(s\mathbf{I} - \frac{\partial s}{\partial\nabla\phi}\nabla\phi\right)\cdot\mathbf{v} - \frac{\mathbf{q}}{T} - \frac{\delta S}{\delta\phi}J\right]d\mathbf{a}, \qquad (2.11)
\end{aligned}
$$

where $\mathbf{n}$ is the unit outward normal vector. The bulk entropy production rate is given by

$$
\frac{dS_{gen}}{dt} = \int_\Omega \left[\frac{\delta S}{\delta e}\left(\sigma_e + 2\eta\mathbf{D} - T\frac{\partial s}{\partial\nabla\phi}\nabla\phi\right) : \nabla\mathbf{v} + \mathbf{q}\cdot\nabla\left(\frac{1}{T}\right) + \nabla\frac{\delta S}{\delta\phi}\cdot J\right]d\mathbf{x}. \qquad (2.12)
$$

The generalized Onsager principle states that this quantity must be nonnegative for nonequilibrium processes. Therefore, we propose the following constitutive equations using the Onsager linear response theory as follows:

$$
J = \mathbf{M}\nabla\frac{\delta S}{\delta\phi}, \quad \sigma_e = T\frac{\partial s}{\partial\nabla\phi}\nabla\phi, \quad \mathbf{q} = D_e(T,\phi)\nabla\frac{1}{T}, \quad D_e = D_0(\phi)T^2, \qquad (2.13)
$$

where $\mathbf{M} > 0$ is the mobility coefficient and $D_0 > 0$ the thermal conductivity constant. So, we deduce that the hydrodynamic phase-field model satisfies the second law of thermodynamics with a positive bulk entropy production rate,

$$
\frac{dS_{gen}}{dt} = \int_\Omega \left(2\eta\frac{1}{T}\mathbf{D} : \mathbf{D} + \frac{D_0}{T^2}|\nabla T|^2 + \mathbf{M}\left|\nabla\frac{\delta S}{\delta\phi}\right|^2\right)d\mathbf{x} \geq 0. \qquad (2.14)
$$

As the system respects the second law of thermodynamics, the phase-field model of nonisothermal two-phase Navier–Stokes flows maintains thermodynamic consistency.

Then, we note that the boundary entropy production rate of the system is given by

$$
\int_{\partial\Omega}\mathbf{n}\cdot\left[\frac{\partial s}{\partial\nabla\phi}\phi_t - \left(s\mathbf{I} - \frac{\partial s}{\partial\nabla\phi}\nabla\phi\right)\cdot\mathbf{v} - \frac{\mathbf{q}}{T} - \frac{\delta S}{\delta\phi}\mathbf{M}\nabla\frac{\delta S}{\delta\phi}\right]d\mathbf{a}. \qquad (2.15)
$$

Since the boundary entropy flux is zero in an insulated system, a set of sufficient physical boundary conditions are given as follows

$$
\mathbf{v}\,|_{\partial\Omega} = 0, \ \frac{\partial s}{\partial\nabla\phi}\cdot\mathbf{n}\,|_{\partial\Omega} = 0, \ \nabla\frac{\delta S}{\delta\phi}\cdot\mathbf{n}\,|_{\partial\Omega} = 0, \ \mathbf{n}\cdot\mathbf{q}\,|_{\partial\Omega} = 0. \qquad (2.16)
$$

Remark 2.1 Based on the Onsager principle, we can derive boundary conditions of the system by budgeting the boundary entropy production rate. Boundary condition (2.16) is obtained by setting sufficient conditions to annihilate the boundary entropy flux (2.15). Other type boundary conditions associated to nonvanishing boundary entropy flux in different applications can be derived as well, which is out of the scope of this study.

Combining boundary condition (2.16) with Eq. (2.5), we obtain the rate of change in the total energy

$$\frac{dE}{dt} = \int_\Omega \left[e_t + \frac{\rho}{2}\left(|\mathbf{v}|^2\right)_t \right] d\mathbf{x} = \int_\Omega \mathbf{b}\cdot\mathbf{v} d\mathbf{x}. \tag{2.17}$$

Note that if $\mathbf{b}$=0, $\frac{dE}{dt} = 0$, namely, the total energy of the system is conserved absent of any external forces. We define the volume of fluid A in domain Ω as

$$V = \int_\Omega \phi d\mathbf{x}. \tag{2.18}$$

Then, volume is guaranteed by

$$\frac{dV}{dt} = \int_\Omega \phi_t d\mathbf{x} = -\int_\Omega \left[\nabla\cdot\mathbf{M}\nabla\frac{\delta S}{\delta\phi} + \nabla\cdot(\phi\mathbf{v}) \right] d\mathbf{x} = 0. \tag{2.19}$$

In summary, the governing system of equations in the hydrodynamic phase field model is consisted of the following equations

$$\begin{cases} \phi_t + \nabla\cdot(\phi\mathbf{v}) = -\nabla\cdot\mathbf{M}\nabla\frac{\delta S}{\delta\phi}, \\ \nabla\cdot\mathbf{v} = 0, \\ \rho\mathbf{v}_t + \rho\nabla\cdot(\mathbf{v}\mathbf{v}) = \nabla\cdot(\sigma_e + 2\eta\mathbf{D} - p\mathbf{I}) + \mathbf{b}, \\ e_t + \nabla\cdot(e\mathbf{v}) = (\sigma_e + 2\eta\mathbf{D}) : \nabla\mathbf{v} - \nabla\cdot\mathbf{q}. \end{cases} \tag{2.20}$$

If the boundary is insulated (adiabatic), the physical boundary conditions are given by (2.16). We note that $\mathbf{M}$, η are functions of (ϕ, T) while $\mathbf{q}$ is a function of $(T, \phi, \nabla T, \nabla\phi)$. In this paper, we assume that $\mathbf{M} > 0$ is a constant and $\eta = \eta_1(T)\phi + \eta_2(T)(1-\phi)$, where viscosity coefficients $\eta_1(T)$, $\eta_2(T)$ have the same property and given by Velzen et al. [27]

$$\eta_{1,2}(T) = A_0 e^{B_0/T}, \tag{2.21}$$

where A_0 and B_0 are constants.

2.3 Internal Energy and Bulk Entropy

In this model, the internal energy density is approximated by an interpolated internal energy from fluid phase A ($\phi = 1$) to fluid phase B ($\phi = 0$) as follows:

$$e(T,\phi) = e_B(T) + p(\phi)L(T) = e_A(T) + (p(\phi) - 1)L(T), \tag{2.22}$$

where $e_A(T)$ and $e_B(T)$ are the classical internal energy density of phase A and phase B, respectively, and $L(T) = e_A(T) - e_B(T)$ measures the difference known as the latent heat, $p(\phi)$ is a monotonic interpolation function that satisfies $p(0) = 0$ and $p(1) = 1$. We assume the internal energy in phase A is higher than that in phase B, so $L(T) > 0$. We note that the bulk Helmholtz free energy can be expressed as

$$f(T,\phi) = e - Ts_0(e,\phi). \tag{2.23}$$

Since $\frac{\partial s_0}{\partial e} = \frac{1}{T}$,

$$\frac{\partial(f/T)}{\partial T} = -\frac{e}{T^2} + \frac{1}{T}\frac{\partial e}{\partial T} - \frac{\partial s_0}{\partial e}\frac{\partial e}{\partial T} = -\frac{e}{T^2}. \tag{2.24}$$

Equation (2.24) allows us to obtain the bulk Helmholtz free energy once the internal energy is given as a function of (T, ϕ).

Form (2.24) and (2.22), we have

$$f(T,\phi) = T\left[-\int_{T_M}^{T}\frac{e(\xi,\phi)}{\xi^2}d\xi + F(\phi)\right]$$
$$= T\left[-\int_{T_M}^{T}\frac{e_A(\xi)}{\xi^2}d\xi - (p(\phi)-1)Q(T) + F(\phi)\right], \tag{2.25}$$

where $Q(T) = \int_{T_M}^{T}\frac{L(\xi)}{\xi^2}d\xi$ is monotonically increasing with respect to T and $Q(T_M) = 0$ at a critical temperature T_M. We choose $F(\phi) = \gamma_2\phi^2(1-\phi)^2$ and $p(\phi) = 30\left(\frac{\phi^5}{5} - \frac{\phi^4}{2} + \frac{\phi^3}{3}\right)$, where γ_2 measures the strength of the repulsive potential [17].

Following the usual practice, we assume $e_A(T) = e_A(T_M) + C_A(T - T_M)$, where T_M is the transition temperature, and $L(T) = L_0$ is the latent heat, where C_A is the specific heat of phase A and $e_A(T_M)$, C_A, T_M, L_0 are constants. Then, e is given explicitly by

$$e(T,\phi) = e_A(T_M) + C_A(T - T_M) + (p(\phi)-1)L_0. \tag{2.26}$$

Equation (2.25) recast into

$$f(T,\phi) = T\big[e_A(T_M) - C_A T_M + (p(\phi)-1)L_0\big]\left(\frac{1}{T} - \frac{1}{T_M}\right)$$
$$-TC_A(\ln T - \ln T_M) + TF(\phi). \tag{2.27}$$

The bulk entropy is then given by

$$s_0(T,\phi) = C_A + [e_A(T_M) - C_A T_M + (p(\phi)-1)L_0]\frac{1}{T_M} + C_A(\ln T - \ln T_M) - F(\phi). \tag{2.28}$$

From (2.26), we obtain T in terms of e:

$$T = \frac{1}{C_A}[e - e_A(T_M) - (p(\phi)-1)L_0] + T_M. \tag{2.29}$$

It follows that

$$s_0(e,\phi) = C_A + \frac{1}{T_M}[e_A(T_M) - C_A T_M + (p(\phi)-1)L_0] + C_A(\ln T - \ln T_M) - F(\phi)$$
$$= C_A\ln[e - e_A(T_M) - (p(\phi)-1)L_0 + C_A T_M] - C_A(\ln C_A + \ln T_M) - F(\phi)$$
$$+ C_A + \frac{1}{T_M}[e_A(T_M) - C_A T_M + (p(\phi)-1)L_0]. \tag{2.30}$$

(2.30) recovers the classical relation

$$\frac{\delta S}{\delta e} = \frac{\partial s_0}{\partial e} = \frac{C_A}{e - e_A(T_M) - (p(\phi)-1)L_0 + C_A T_M} = \frac{1}{T}. \tag{2.31}$$

The conformational entropy is given by

$$s_1(\nabla\phi) = -\frac{\gamma_1}{2}|\nabla\phi|^2, \tag{2.32}$$

where γ_1 measures the strength of the conformational entropy. The total entropy S of the system takes the following form

$$S(e,\phi,\nabla\phi) = \int_\Omega\left[-\frac{\gamma_1}{2}|\nabla\phi|^2 + s_0(e,\phi)\right]d\mathbf{x}. \tag{2.33}$$

2.4 Non-dimensionalization

We use a characteristic length scale l_0, time scale t_0, density scale ρ_0 and temperature scale T_0 to nondimensionalize the physical variables and parameters as follows:

$$\begin{aligned}
&\tilde{\phi} = \phi, \quad \tilde{x} = \frac{x}{l_0}, \quad \tilde{y} = \frac{y}{l_0}, \quad \tilde{t} = \frac{t}{t_0}, \quad \tilde{\rho} = \frac{\rho}{\rho_0}, \quad \tilde{T} = \frac{T}{T_0}, \quad \tilde{\mathbf{v}} = \frac{t_0\mathbf{v}}{l_0}, \quad \tilde{\mathbf{M}} = \frac{\rho_0\mathbf{M}}{t_0T_0},\\
&\frac{\delta\tilde{S}}{\delta\phi} = \frac{t_0^2T_0}{\rho_0l_0^2}\frac{\delta S}{\delta\phi}, \quad \tilde{\sigma}_e = \frac{t_0^2\sigma_e}{\rho_0l_0^2}, \quad \tilde{\eta} = \frac{1}{Re} = \frac{t_0\eta}{\rho_0l_0^2}, \quad \tilde{p} = \frac{t_0^2p}{\rho_0l_0^2}, \quad \tilde{\mathbf{b}} = \frac{t_0^2\mathbf{b}}{\rho_0l_0}, \quad \tilde{e} = \frac{t_0^2e}{\rho_0l_0^2},\\
&\tilde{D}_0 = \frac{t_0^3T_0D_0}{\rho_0l_0^4}, \quad \tilde{\gamma_1} = \frac{T_0t_0^2\gamma_1}{\rho_0l_0^4}, \quad \tilde{\gamma_2} = \frac{T_0t_0^2\gamma_2}{\rho_0l_0^2}, \quad \tilde{C_A} = \frac{T_0t_0^2C_A}{\rho_0l_0^2}, \quad \tilde{A}_0 = \frac{t_0A_0}{\rho_0l_0^2},\\
&\tilde{T}_M = \frac{T_M}{T_0}, \quad \tilde{e}_A = \frac{t_0^2e_A}{\rho_0l_0^2}, \quad \tilde{L}_0 = \frac{t_0^2L_0}{\rho_0l_0^2}, \quad \tilde{s_0} = \frac{t_0^2T_0}{\rho_0l_0^2}s_0, \quad \tilde{S} = \frac{t_0^2T_0}{\rho_0l_0^5}S.
\end{aligned} \tag{2.34}$$

where Re denote the Reynolds number. After we drop the $\tilde{}$ on the dimensionless variables and the parameters, we have the dimensionless total entropy below

$$S(e,\phi,\nabla\phi) = \int_\Omega [s_0(e,\phi) + s_1(\nabla\phi)]d\mathbf{x} = \int_\Omega \left[-\frac{\gamma_1}{2}|\nabla\phi|^2 + s_0(e,\phi)\right]d\mathbf{x}, \tag{2.35}$$

and the dimensionless governing equations as follows

$$\begin{cases}
\phi_t + \nabla\cdot(\phi\mathbf{v}) = -\nabla\cdot\mathbf{M}\nabla\frac{\delta S}{\delta\phi},\\
\nabla\cdot\mathbf{v} = 0,\\
\rho\mathbf{v}_t + \rho\nabla\cdot(\mathbf{v}\mathbf{v}) = \nabla\cdot(\sigma_e + 2\eta\mathbf{D} - p\mathbf{I}) + \mathbf{b},\\
e_t + \nabla\cdot(e\mathbf{v}) = (\sigma_e + 2\eta\mathbf{D}) : \nabla\mathbf{v} - \nabla\cdot\left(D_0T^2\nabla\frac{1}{T}\right),
\end{cases} \tag{2.36}$$

where $\eta = \frac{1}{Re}$.

Next, we develop structure preserving numerical approximations to the governing system of equations in a bounded domain. We present the results in 2-dimensional spatial domains. The results apply to 3-dimensional domains as well.

3 Notation and Useful Lemmas

In this section, we introduce some notations, lemmas and definitions of grid functions in two-dimensional space. Firstly, we denote the computational domain by $\Omega = [0, L_x] \times [0, L_y]$ with $L_x = h_x \times N_x$, $L_y = h_y \times N_y$, where N_x, N_y are positive integers and h_x, h_y are mesh sizes. We define the following sets for various grid points:

$$\begin{aligned}
E_x &= \left\{x_{i+\frac{1}{2}} | i = 0, 1, \ldots, N_x\right\}, C_x = \{x_i | i = 1, 2, \ldots, N_x\},\\
&\quad C_{\bar{x}} = \{x_i | i = 0, 1, \ldots, N_x + 1\},\\
E_y &= \left\{y_{j+\frac{1}{2}} | j = 0, 1, \ldots, N_y\right\}, C_y = \{y_j | j = 1, 2, \ldots, N_y\},\\
&\quad C_{\bar{y}} = \{y_j | j = 0, 1, \ldots, N_y + 1\},
\end{aligned}$$

where $x_l = \left(l - \frac{1}{2}\right)h_x$, $y_l = \left(l - \frac{1}{2}\right)h_y$, l can take on integer or half-integer values. The elements of E_x, E_y are called edge-centered points, the elements of C_x, C_y, $C_{\bar{x}}$, $C_{\bar{y}}$ are called

cell-centered points and the two points belonging to $C_{\bar{x}}\backslash C_x$ are called ghost points. In this paper, we chose $h_x = h_y = h$ for simplicity.

We define the following discrete function spaces

$$\mathcal{C}_{x\times y} = \{\phi : C_x \times C_y \to \mathbb{R}\}, \mathcal{C}_{\bar{x}\times y} = \{\phi : C_{\bar{x}} \times C_y \to \mathbb{R}\}, \mathcal{C}_{x\times \bar{y}} = \{\phi : C_x \times C_{\bar{y}} \to \mathbb{R}\},$$
$$\mathcal{C}_{\bar{x}\times \bar{y}} = \{\phi : C_{\bar{x}} \times C_{\bar{y}} \to \mathbb{R}\}, \varepsilon^{ew}_{x\times y} = \{u : E_x \times C_y \to \mathbb{R}\}, \varepsilon^{ew}_{x\times \bar{y}} = \{u : E_x \times C_{\bar{y}} \to \mathbb{R}\},$$
$$\varepsilon^{ns}_{x\times y} = \{v : C_x \times E_y \to \mathbb{R}\}, \varepsilon^{ns}_{\bar{x}\times y} = \{v : C_{\bar{x}} \times E_{\bar{y}} \to \mathbb{R}\}, \nu_{x\times y} = \{f : E_x \times E_y \to \mathbb{R}\}.$$

The functions in $\mathcal{C}_{x\times y}, \mathcal{C}_{\bar{x}\times y}, \mathcal{C}_{x\times \bar{y}}, \mathcal{C}_{\bar{x}\times \bar{y}}$ are called cell centered discrete functions, the functions in $\nu_{x\times y}$ are called vertex centered discrete functions, the functions in $\varepsilon^{ew}_{x\times y}, \varepsilon^{ew}_{x\times \bar{y}}$ and $\varepsilon^{ns}_{x\times y}, \varepsilon^{ns}_{\bar{x}\times y}$ are called east-west and north-south edge centered discrete functions, respectively.

3.1 Definitions of Operators

First, we assume ϕ, ψ are cell centered functions, u, r are east-west edge centered functions, v, w are north-south edge centered functions and f, g are vertex centered functions. Then, $\phi, \psi \in \mathcal{C}_{x\times y} \cup \mathcal{C}_{\bar{x}\times y} \cup \mathcal{C}_{x\times \bar{y}} \cup \mathcal{C}_{\bar{x}\times \bar{y}}$, $u, r \in \varepsilon^{ew}_{x\times y} \cup \varepsilon^{ew}_{x\times \bar{y}}$, $v, w \in \varepsilon^{ns}_{x\times y} \cup \varepsilon^{ns}_{\bar{x}\times y}$, $f, g \in \nu_{x\times y}$.

Next, we denote the east-west-edge-to-center average and difference operators as a_x, d_x, defined by

$$a_x u_{i,j} := \frac{1}{2}\left(u_{i+\frac{1}{2},j} + u_{i-\frac{1}{2},j}\right), \quad d_x u_{i,j} := \frac{1}{h_x}\left(u_{i+\frac{1}{2},j} - u_{i-\frac{1}{2},j}\right),$$
$$a_x f_{i,j+\frac{1}{2}} := \frac{1}{2}\left(f_{i+\frac{1}{2},j+\frac{1}{2}} + f_{i-\frac{1}{2},j+\frac{1}{2}}\right), \quad d_x f_{i,j+\frac{1}{2}} := \frac{1}{h_x}\left(f_{i+\frac{1}{2},j+\frac{1}{2}} - f_{i-\frac{1}{2},j+\frac{1}{2}}\right). \tag{3.1}$$

The north-south-edge-to-center average and difference operators are defined as a_y, d_y,

$$a_y v_{i,j} := \frac{1}{2}\left(v_{i,j+\frac{1}{2}} + u_{i,j-\frac{1}{2}}\right), \quad d_y v_{i,j} := \frac{1}{h_y}\left(v_{i,j+\frac{1}{2}} - v_{i,j-\frac{1}{2}}\right),$$
$$a_y f_{i+\frac{1}{2},j} := \frac{1}{2}\left(f_{i+\frac{1}{2},j+\frac{1}{2}} + f_{i+\frac{1}{2},j-\frac{1}{2}}\right), \quad d_y f_{i+\frac{1}{2},j} := \frac{1}{h_y}\left(f_{i+\frac{1}{2},j+\frac{1}{2}} - f_{i+\frac{1}{2},j-\frac{1}{2}}\right). \tag{3.2}$$

The center-to-east-west-edge average and difference operators are defined as A_x, D_x,

$$A_x \phi_{i+\frac{1}{2},j} := \frac{1}{2}(\phi_{i+1,j} + \phi_{i,j}), \quad D_x \phi_{i+\frac{1}{2},j} := \frac{1}{h_x}(\phi_{i+1,j} - \phi_{i,j}),$$
$$A_x v_{i+\frac{1}{2},j+\frac{1}{2}} := \frac{1}{2}\left(v_{i+1,j+\frac{1}{2}} + v_{i,j+\frac{1}{2}}\right), \quad D_x v_{i+\frac{1}{2},j+\frac{1}{2}} := \frac{1}{h_x}\left(v_{i+1,j+\frac{1}{2}} - v_{i,j+\frac{1}{2}}\right). \tag{3.3}$$

The center-to-north-south-edge average and difference operators are defined as A_y, D_y,

$$A_y \phi_{i,j+\frac{1}{2}} := \frac{1}{2}(\phi_{i,j+1} + \phi_{i,j}), \quad D_y \phi_{i,j+\frac{1}{2}} := \frac{1}{h_y}(\phi_{i,j+1} - \phi_{i,j}),$$
$$A_y u_{i+\frac{1}{2},j+\frac{1}{2}} := \frac{1}{2}\left(u_{i+\frac{1}{2},j+1} + u_{i+\frac{1}{2},j}\right), \quad D_y u_{i+\frac{1}{2},j+\frac{1}{2}} := \frac{1}{h_y}\left(u_{i+\frac{1}{2},j+1} - u_{i+\frac{1}{2},j}\right). \tag{3.4}$$

3.2 Boundary Condition Treatments

We assume cell centered functions ϕ, ψ satisfy Neumann boundary conditions and edge centered functions u, v satisfy Dirichlet boundary conditions. Then, cell centered functions $\phi \in \mathcal{C}_{\bar{x}\times\bar{y}}$ is said to satisfy homogeneous Neumann boundary conditions if and only if

$$\begin{aligned} &\phi_{0,j} = \phi_{1,j}, \quad \phi_{N_x,j} = \phi_{N_x+1,j}, \quad j = 1, 2, \ldots, N_y; \\ &\phi_{i,0} = \phi_{i,1}, \quad \phi_{i,N_y} = \phi_{i,N_y+1}, \quad i = 0, 1, \ldots, N_x + 1. \end{aligned} \tag{3.5}$$

The edge centered functions $u \in \varepsilon^{ew}_{x\times\bar{y}}$, $v \in \varepsilon^{ns}_{\bar{x}\times y}$ are said to satisfy homogeneous Dirichlet boundary conditions if and only if

$$\begin{aligned} &u_{\frac{1}{2},j} = u_{N_x+\frac{1}{2},j} = 0, \quad j = 1, 2, \ldots, N_y, \\ &A_y u_{i+\frac{1}{2},\frac{1}{2}} = A_y u_{i+\frac{1}{2},N_y+\frac{1}{2}} = 0, \quad i = 0, 1, 2, \ldots, N_x, \\ &v_{i,\frac{1}{2}} = v_{i,N_y+\frac{1}{2}} = 0, \quad i = 1, 2, \ldots, N_x, \\ &A_x v_{\frac{1}{2},j+\frac{1}{2}} = A_x v_{N_x+\frac{1}{2},j+\frac{1}{2}} = 0, \quad j = 0, 1, 2, \ldots, N_y. \end{aligned} \tag{3.6}$$

3.3 Inner Products and Norms

We denote the discrete Laplacian operator $\Delta_h : \varepsilon^{ew}_{x\times\bar{y}} \cup \varepsilon^{ns}_{\bar{x}\times y} \cup \mathcal{C}_{\bar{x}\times\bar{y}} \longrightarrow \varepsilon^{ew}_{x\times y} \cup \varepsilon^{ns}_{x\times y} \cup \mathcal{C}_{x\times y}$, defined as

$$\Delta_h u = D_x(d_x u) + d_y(D_y u), \ \Delta_h v = d_x(D_x v) + D_y(d_y v), \ \Delta_h \phi = d_x(D_x \phi) + d_y(D_y \phi), \tag{3.7}$$

and the discrete divergence operator defined as $\nabla_h \cdot : \varepsilon^{ew}_{x\times\bar{y}} \cup \varepsilon^{ns}_{\bar{x}\times y} \longrightarrow \mathcal{C}_{x\times y}$,

$$\nabla_h \cdot \mathbf{v} = d_x u + d_y v; \tag{3.8}$$

and the discrete gradient operator $\nabla_h : \mathcal{C}_{\bar{x}\times\bar{y}} \longrightarrow \varepsilon^{ew}_{x\times y} \cup \varepsilon^{ns}_{x\times y}$,

$$\nabla_h \phi = (D_x \phi, D_y \phi). \tag{3.9}$$

In addition, we define the following discrete inner products

$$\begin{aligned} &(\phi, \psi)_2 := h_x h_y \sum_{i=1}^{N_x} \sum_{j=1}^{N_y} \phi_{i,j} \psi_{i,j}, \\ &[u, r]_{ew} := (a_x(ur), 1)_2 = \frac{1}{2} h_x h_y \sum_{i=1}^{N_x} \sum_{j=1}^{N_y} \left(u_{i+\frac{1}{2},j} r_{i+\frac{1}{2},j} + u_{i-\frac{1}{2},j} r_{i-\frac{1}{2},j} \right), \\ &[v, w]_{ns} := (a_y(vw), 1)_2 = \frac{1}{2} h_x h_y \sum_{i=1}^{N_x} \sum_{j=1}^{N_y} \left(v_{i,j+\frac{1}{2}} w_{i,j+\frac{1}{2}} + v_{i,j-\frac{1}{2}} w_{i,j-\frac{1}{2}} \right), \\ &(f, g)_{vc} := (a_x(a_y(fg)), 1)_2, (\nabla_h \phi, \nabla_h \psi) := [D_x \phi, D_x \psi]_{ew} + [D_y \phi, D_y \psi]_{ns}. \end{aligned} \tag{3.10}$$

Then, their corresponding norms are given as follows

$$\|\phi\|_2 := (\phi, \phi)_2^{\frac{1}{2}}, \quad \|u\|_{ew} := [u, u]_{ew}^{\frac{1}{2}}, \quad \|v\|_{ns} := [v, v]_{ns}^{\frac{1}{2}}, \quad \|f\|_{vc} := (f, f)_{vc}^{\frac{1}{2}}. \tag{3.11}$$

For $\phi \in \mathcal{C}_{x\times y} \cup \mathcal{C}_{\bar{x}\times y} \cup \mathcal{C}_{x\times \bar{y}} \cup \mathcal{C}_{\bar{x}\times \bar{y}}$ we define $\|\nabla\phi\|_2$ as

$$\|\nabla\phi\|_2^2 := \|D_x\phi\|_{ew}^2 + \|D_y\phi\|_{ns}^2. \tag{3.12}$$

For the edge-centered velocity vector $\mathbf{v} = (u, v), u \in \varepsilon_{x\times\bar{y}}^{ew}, v \in \varepsilon_{\bar{x}\times y}^{ns}$, we define $\|\mathbf{v}\|_2, \|\nabla\mathbf{v}\|_2$ as

$$\begin{aligned} &\|\mathbf{v}\|_2^2 := \|u\|_{ew}^2 + \|v\|_{ns}^2, \quad \|\nabla\mathbf{v}\|_2^2 := \|d_x u\|_2^2 + \|D_y u\|_{vc}^2 + \|D_x v\|_{vc}^2 + \|d_y v\|_2^2, \\ &\|\mathbf{D}\|_2^2 := \|d_x u\|_2^2 + \frac{1}{2}\|D_y u\|_{vc}^2 + \frac{1}{2}\|D_x v\|_{vc}^2 + (D_y u, D_x v)_{vc} + \|d_y v\|_2^2. \end{aligned} \tag{3.13}$$

where $\mathbf{D} = \frac{1}{2}(\nabla\mathbf{v} + \nabla\mathbf{v}^T)$. We also introduce discrete $\|\cdot\|_\infty$ norm, $\|\cdot\|_p$ norm $(1 \le p < \infty)$ as follows:

$$\|\phi\|_\infty := max_{i,j}|\phi_{i,j}|, \quad \|\phi\|_p := (|\phi|^p, 1)^{\frac{1}{p}}. \tag{3.14}$$

Now, we list some useful lemmas:

Lemma 3.1 *For $\phi, \psi \in \mathcal{C}_{\bar{x}\times\bar{y}}$ satisfying the discrete homogeneous Neumann boundary condition, the following summation by parts formulas can be derived:*

$$-(\Delta_h\phi, \psi)_2 = (\nabla_h\phi, \nabla_h\psi)_2. \tag{3.15}$$

Lemma 3.2 *For $\phi \in \mathcal{C}_{\bar{x}\times\bar{y}}$ satisfying the discrete homogeneous Neumann boundary condition, $\mathbf{v} = (u, v), u \in \varepsilon_{x\times\bar{y}}^{ew}, v \in \varepsilon_{\bar{x}\times y}^{ns}$ satisfying the homogeneous Dirichlet boundary condition, the following summation by parts formulas can be derived:*

$$\begin{aligned} &[A_x\phi, u]_{ew} = (\phi, a_x u)_2, \quad [A_y\phi, v]_{ns} = (\phi, a_y v)_2, \\ &[D_x\phi, u]_{ew} = -(\phi, d_x u)_2, \quad [D_y\phi, v]_{ns} = -(\phi, d_y v)_2. \end{aligned} \tag{3.16}$$

Lemma 3.3 *For $f \in v_{x\times y}$ satisfying the discrete homogeneous Dirichlet boundary condition and $u \in \varepsilon_{x\times\bar{y}}^{ew}, v \in \varepsilon_{\bar{x}\times y}^{ns}$, the following formulas can be derived:*

$$[a_y f, u]_{ew} = (f, A_y u)_{vc}, \quad [a_x f, v]_{ns} = (f, A_x v)_{vc}. \tag{3.17}$$

Lemma 3.4 *For $u \in \varepsilon_{x\times\bar{y}}^{ew}, v \in \varepsilon_{\bar{x}\times y}^{ns}$ satisfying the discrete homogeneous Dirichlet boundary condition and $f \in v_{x\times y}$, the following formulas can be derived:*

$$[d_y f, u]_{ew} = -(f, D_y u)_{vc}, \quad [d_x f, v]_{ns} = -(f, D_x v)_{vc}. \tag{3.18}$$

4 Structure-Preserving Numerical Approximations

The hydrodynamic model satisfies an energy dissipation law. We would like to develop second order structure preserving schemes in time for the incompressible model to preserve the entropy production rate. We proceed with the entropy quadratization (EQ) method.

4.1 Reformulation of the System of Equations Using EQ Methods

To use the EQ method to design the numerical scheme, we need to reformulate the model equation. First, we introduce an auxiliary variable

$$q = \sqrt{-s_0 - \gamma_2\phi^2 - \gamma_3 e^2 + C_0}, \tag{4.1}$$

where C_0 is a positive constants large enough to ensure that q is real in physically accessible range of the absolute temperature T. So, the system entropy (2.35) is given by a quadratic functional

$$S = \int_\Omega s d\mathbf{x} = \int_\Omega \left(-\frac{\gamma_1}{2}|\nabla\phi|^2 - q^2 - \gamma_2\phi^2 - \gamma_3 e^2 + C_0 \right) d\mathbf{x}. \tag{4.2}$$

From (2.30), we have

$$\begin{aligned} q_\phi = \frac{\partial q}{\partial \phi} &= \frac{-\frac{\partial s_0}{\partial \phi} - 2\gamma_2\phi}{2\sqrt{-s_0 - \gamma_2\phi^2 - \gamma_3 e^2 + C_0}} \\ &= \frac{-\frac{L_0}{T_M}p'(\phi) + \frac{C_A L_0 p'(\phi)}{e - e_A(T_M) - (p(\phi)-1)L_0 + C_A T_M} + F'(\phi) - 2\gamma_2\phi}{2\sqrt{-s_0 - \gamma_2\phi^2 - \gamma_3 e^2 + C_0}}, \end{aligned} \tag{4.3}$$

and

$$q_e = \frac{\partial q}{\partial e} = \frac{-\frac{\partial s_0}{\partial e} - 2\gamma_3 e}{2\sqrt{-s_0 - \gamma_2\phi^2 - \gamma_3 e^2 + C_0}} = -\frac{\frac{1}{\frac{1}{C_A}[e - e_A(T_M) - (p(\phi)-1)L_0] + T_M} + 2\gamma_3 e}{2\sqrt{-s_0 - \gamma_2\phi^2 - \gamma_3 e^2 + C_0}}. \tag{4.4}$$

It follows that

$$\frac{\delta S}{\delta e} = -2qq_e - 2\gamma_3 e = \frac{1}{\frac{1}{C_A}[e - e_A(T_M) - (p(\phi)-1)L_0] + T_M} = \frac{1}{T}. \tag{4.5}$$

Then, we reformulate equations (2.36) into the following augmented system:

$$\begin{cases} \phi_t + \nabla\cdot(\phi\mathbf{v}) = -\nabla\cdot\mathbf{M}\nabla(\gamma_1\Delta\phi - 2qq_\phi - 2\gamma_2\phi), \\ \nabla\cdot\mathbf{v} = 0, \\ \rho\mathbf{v}_t + \rho\nabla\cdot(\mathbf{v}\mathbf{v}) = \nabla\cdot(2\eta\mathbf{D}) - \nabla p + \nabla\cdot\sigma_e + \mathbf{b}, \\ e_t + \nabla\cdot(e\mathbf{v}) = (\sigma_e + 2\eta\mathbf{D}) : \nabla\mathbf{v} + 2\nabla\cdot(D_e\nabla(qq_e + \gamma_3 e)), \\ q_t = q_\phi\phi_t + q_e e_t. \end{cases} \tag{4.6}$$

where

$$\begin{aligned} &q_\phi = \frac{\partial q}{\partial \phi}, \quad q_e = \frac{\partial q}{\partial e}, \quad \sigma_e = -T\gamma_1\nabla\phi\nabla\phi = \frac{\gamma_1\nabla\phi\nabla\phi}{2(qq_e + \gamma_3 e)}, \\ &D_e = D_0 T^2 = D_0\left(\frac{1}{C_A}[e - e_A(T_M) - (p(\phi)-1)L_0] + T_M\right)^2, \\ &\eta = A_0 e^{\frac{B_0}{T}} = A_0 e^{-2B_0(qq_e + \gamma_3 e)}. \end{aligned} \tag{4.7}$$

Next, we examine the entropy production rate of the reformulated system equations. Note that

$$\frac{\delta S}{\delta \phi} = \gamma_1\Delta\phi - 2qq_\phi - 2\gamma_2\phi, \quad \frac{\delta S}{\delta e} = -2qq_e - 2\gamma_3 e = \frac{1}{T}. \tag{4.8}$$

The entropy production rate is calculated as follows

$$\begin{aligned}
\frac{dS}{dt} &= \int_\Omega \left(\phi_t \frac{\delta S}{\delta \phi} + \frac{\delta S}{\delta e} e_t\right) d\mathbf{x} = \int_\Omega (-\gamma_1 \nabla\phi \nabla\phi_t - 2qq_t - 2\gamma_2 \phi\phi_t - 2\gamma_3 e e_t) d\mathbf{x} \\
&= \int_\Omega \left[\phi_t(\gamma_1 \Delta\phi - 2\gamma_2\phi) - 2qq_\phi \left(-\nabla\cdot\mathbf{M}\nabla\frac{\delta S}{\delta\phi} - \nabla\cdot(\phi\mathbf{v})\right) - 2(qq_e + \gamma_3 e)e_t\right] d\mathbf{x} \\
&= \int_\Omega \left[\mathbf{M}\left|\nabla\frac{\delta S}{\delta\phi}\right|^2 + \frac{\delta S}{\delta e}\sigma_e : \nabla\mathbf{v} + \frac{1}{T}2\eta\mathbf{D} : \nabla\mathbf{v} + D_e\left|\nabla\frac{\delta S}{\delta e}\right|^2\right. \\
&\quad \left. - \left[\nabla\cdot(\phi\mathbf{v})\frac{\delta S}{\delta\phi} + \nabla\cdot(e\mathbf{v})\frac{\delta S}{\delta e}\right]\right] d\mathbf{x} - \int_{\partial\Omega} \mathbf{n}\cdot\left(\frac{\delta S}{\delta e} D_e \nabla\frac{\delta S}{\delta e}\right) d\mathbf{a} \\
&= \int_\Omega \mathbf{M}\left|\nabla\frac{\delta S}{\delta\phi}\right|^2 + \frac{\delta S}{\delta e}\sigma_e : \nabla\mathbf{v} + \frac{1}{T}2\eta\mathbf{D} : \nabla\mathbf{v} + D_e\left|\nabla\frac{\delta S}{\delta e}\right|^2 \\
&\quad - \left[\left(\frac{\delta S}{\delta\phi}\phi + \frac{\delta S}{\delta e}e\right)\mathbf{I} : \nabla\mathbf{v} + \left(\frac{\delta S}{\delta\phi}\nabla\phi + \frac{\delta S}{\delta e}\nabla e\right)\cdot\mathbf{v}\right] d\mathbf{x} - \int_{\partial\Omega}\mathbf{n}\cdot\left(\frac{\delta S}{\delta e} D_e\nabla\frac{\delta S}{\delta e}\right) d\mathbf{a} \\
&= \int_\Omega \left(2\eta\frac{1}{T}\mathbf{D} : \mathbf{D} + D_e\left|\frac{\delta S}{\delta e}\right|^2 + \mathbf{M}\left|\nabla\frac{\delta S}{\delta\phi}\right|^2\right) d\mathbf{x} - \int_{\partial\Omega}\mathbf{n}\cdot\left(\frac{\delta S}{\delta e} D_e\nabla\frac{\delta S}{\delta e}\right) d\mathbf{a}. \quad (4.9)
\end{aligned}$$

where the physical boundary conditions in (2.16) are applied. From the above result, we obtain the positive entropy production rate of the reformulated system (4.6) as follows

$$\frac{dS_{gen}}{dt} = \int_\Omega \left(2\eta\frac{1}{T}\mathbf{D} : \mathbf{D} + D_e\left|\frac{\delta S}{\delta e}\right|^2 + \mathbf{M}\left|\nabla\frac{\delta S}{\delta\phi}\right|^2\right) d\mathbf{x} \geq 0. \quad (4.10)$$

Note that the following identity is used

$$-\left(\frac{\delta S}{\delta e}\nabla e + \frac{\delta S}{\delta\phi}\nabla\phi\right)\cdot\mathbf{v} = \left(-\frac{\partial s}{\partial\nabla\phi}\nabla\phi\right) : \nabla\mathbf{v} - \nabla\cdot\left[\left(s\mathbf{I} - \frac{\partial s}{\partial\nabla\phi}\nabla\phi\right)\cdot\mathbf{v}\right]. \quad (4.11)$$

The result indicates that the EQ reformulated system retains thermodynamic consistency. Next, we discuss the temporal discretization of the EQ reformulated system.

4.2 Temporal Discretization

We discretize the EQ reformulated PDE system (4.6) using the Crank–Nicolson method with some terms extrapolated in time. We adopt the following notations

$$\delta_t(\cdot)^{n+\frac{1}{2}} = \frac{1}{\Delta t}((\cdot)^{n+1} - (\cdot)^n), \qquad \overline{(\cdot)}^{n+\frac{1}{2}} = \frac{1}{2}(3(\cdot)^n - (\cdot)^{n-1}). \quad (4.12)$$

A second order nonlinear implicit semi-discrete scheme is given below.

Scheme 1 **(EQ Scheme)**

$$\begin{cases} \delta_t \phi^{n+\frac{1}{2}} + \nabla \cdot \left(\bar{\phi}^{n+\frac{1}{2}} \mathbf{v}^{n+\frac{1}{2}} \right) = -\nabla \cdot \mathbf{M} \nabla \left(\gamma_1 \Delta \phi^{n+\frac{1}{2}} - 2 q^{n+\frac{1}{2}} \bar{q}_\phi^{n+\frac{1}{2}} - 2\gamma_2 \phi^{n+\frac{1}{2}} \right), \\ \nabla \cdot \mathbf{v}^{n+\frac{1}{2}} = 0, \\ \rho \delta_t \mathbf{v}^{n+\frac{1}{2}} + \rho \nabla \cdot \left(\bar{\mathbf{v}}^{n+\frac{1}{2}} \mathbf{v}^{n+\frac{1}{2}} \right) = \nabla \cdot \left(2\eta^{n+\frac{1}{2}} \mathbf{D}^{n+\frac{1}{2}} \right) - \nabla p^{n+\frac{1}{2}} + \nabla \cdot \sigma_e^{n+\frac{1}{2}} + \mathbf{b}^{n+\frac{1}{2}}, \\ \delta_t e^{n+\frac{1}{2}} + \nabla \cdot \left(\bar{e}^{n+\frac{1}{2}} \mathbf{v}^{n+\frac{1}{2}} \right) = \sigma_e^{n+\frac{1}{2}} : \nabla \mathbf{v}^{n+\frac{1}{2}} + 2\eta^{n+\frac{1}{2}} \mathbf{D}^{n+\frac{1}{2}} : \nabla \mathbf{v}^{n+\frac{1}{2}} \\ +2\nabla \cdot \left[\bar{D}_e^{n+\frac{1}{2}} \nabla \left(q^{n+\frac{1}{2}} \bar{q}_e^{n+\frac{1}{2}} + \gamma_3 e^{n+\frac{1}{2}} \right) \right], \\ \delta_t q^{n+\frac{1}{2}} = \bar{q}_\phi^{n+\frac{1}{2}} \delta_t \phi^{n+\frac{1}{2}} + \bar{q}_e^{n+\frac{1}{2}} \delta_t e^{n+\frac{1}{2}}, \end{cases} \tag{4.13}$$

where

$$\begin{aligned} \sigma_e^{n+\frac{1}{2}} &= \frac{\gamma_1 \nabla \phi^{n+\frac{1}{2}} \nabla \phi^{n+\frac{1}{2}}}{2 \left(q^{n+\frac{1}{2}} \bar{q}_e^{n+\frac{1}{2}} + \gamma_3 e^{n+\frac{1}{2}} \right)}, \\ \bar{D}_e^{n+\frac{1}{2}} &= D_0 \left(\frac{1}{C_A} \left[\bar{e}^{n+\frac{1}{2}} - e_A(T_M) - \left(p \left(\bar{\phi}^{n+\frac{1}{2}} \right) - 1 \right) L_0 \right] + T_M \right)^2, \\ \eta^{n+\frac{1}{2}} &= A_0 e^{\left(\frac{B_0}{T} \right)^{n+\frac{1}{2}}} = A_0 e^{-2B_0 \left(q^{n+\frac{1}{2}} \bar{q}_e^{n+\frac{1}{2}} + \gamma_3 e^{n+\frac{1}{2}} \right)}. \end{aligned} \tag{4.14}$$

The physical boundary conditions are discretized as follows

$$\mathbf{v}^n|_{\partial\Omega} = 0, \mathbf{n} \cdot \frac{\partial s}{\partial \nabla \phi}^n|_{\partial\Omega} = 0, \mathbf{n} \cdot \nabla \frac{\delta S}{\delta \phi}^n|_{\partial\Omega} = 0, \mathbf{n} \cdot \nabla \phi^n = 0, \mathbf{n} \cdot \mathbf{q}^n|_{\partial\Omega} = 0 \ (n = 0, 1, \cdots, N). \tag{4.15}$$

Next, we prove that Scheme 1 not only preserves the total energy and volume, but also preserves the positive entropy production rate. We denote

$$\begin{aligned} \frac{\delta S}{\delta \phi}^{n+\frac{1}{2}} &= \gamma_1 \Delta \phi^{n+\frac{1}{2}} - 2 q^{n+\frac{1}{2}} \bar{q}_\phi^{n+\frac{1}{2}} - 2\gamma_2 \phi^{n+\frac{1}{2}}, \\ \frac{\delta S}{\delta e}^{n+\frac{1}{2}} &= -2 q^{n+\frac{1}{2}} \bar{q}_e^{n+\frac{1}{2}} - 2\gamma_3 e^{n+\frac{1}{2}} = \left(\frac{1}{T} \right)^{n+\frac{1}{2}}. \end{aligned} \tag{4.16}$$

Theorem 4.1 *1. Under boundary conditions (4.15), Scheme 1 preserves the total energy balance*

$$E^{n+1} - E^n = \int_\Omega \mathbf{b}^{n+\frac{1}{2}} \cdot \mathbf{v}^{n+\frac{1}{2}} d\mathbf{x}, \tag{4.17}$$

where

$$E^n = \int_\Omega \left[e^n + \frac{\rho}{2} |\mathbf{v}^n|^2 \right] d\mathbf{x}. \tag{4.18}$$

If $\mathbf{b}^{n+\frac{1}{2}}=0$, $E^{n+1}=E^n$, *i.e., Scheme 1 preserves the total energy conservation.*

2. *Scheme 1 preserves the volume of fluid A:*

$$V^{n+1}=V^n, \tag{4.19}$$

where

$$V^n=\int_\Omega \phi^n d\mathbf{x}. \tag{4.20}$$

3. *Scheme 1 preserves the positive entropy production rate,*

$$\begin{aligned}&\frac{S^{n+1}-S^n}{\Delta t}|_{gen}\\&=\int_\Omega\left[\mathbf{M}\left(\nabla\frac{\delta S}{\delta\phi}^{n+\frac{1}{2}}\right)^2+2\eta^{n+\frac{1}{2}}\left(\frac{1}{T}\right)^{n+\frac{1}{2}}\mathbf{D}^{n+\frac{1}{2}}:\mathbf{D}^{n+\frac{1}{2}}+\bar{D}_e^{n+\frac{1}{2}}\left|\nabla\frac{\delta S}{\delta e}^{n+\frac{1}{2}}\right|^2\right]\\&d\mathbf{x}\geq 0,\end{aligned} \tag{4.21}$$

where

$$S^n=\int_\Omega\left[-|q^n|^2-\gamma_2|\phi^n|^2-\gamma_3|e^n|^2-\frac{\gamma_1}{2}|\nabla\phi^n|^2+C_0\right]d\mathbf{x}. \tag{4.22}$$

Proof Since $\nabla\cdot\bar{\mathbf{v}}=0$, we have

$$\begin{aligned}\nabla\cdot(\bar{\mathbf{v}}\mathbf{v})\cdot\mathbf{v}&=(\bar{\mathbf{v}}\cdot\nabla\mathbf{v}+\mathbf{v}\nabla\cdot\bar{\mathbf{v}})\cdot\mathbf{v}=\frac{1}{2}(\bar{\mathbf{v}}\cdot\nabla\mathbf{v}+\bar{\mathbf{v}}\cdot\nabla\mathbf{v}+\mathbf{v}\nabla\cdot\bar{\mathbf{v}})\cdot\mathbf{v}\\&=\frac{1}{2}[\nabla\cdot(|\mathbf{v}|^2\bar{\mathbf{v}})].\end{aligned} \tag{4.23}$$

Taking the inner product of (4.13-3) with $\mathbf{v}^{n+\frac{1}{2}}$, we obtain

$$\begin{aligned}&\rho\frac{\mathbf{v}^{n+1}-\mathbf{v}^n}{\Delta t}\frac{\mathbf{v}^{n+1}+\mathbf{v}^n}{2}+\nabla\cdot\left[\left(\frac{\rho}{2}|\mathbf{v}^{n+\frac{1}{2}}|^2\right)\bar{\mathbf{v}}^{n+\frac{1}{2}}\right]\\&=\mathbf{v}^{n+\frac{1}{2}}\cdot\left[\nabla\cdot\left(\sigma_e^{n+\frac{1}{2}}+2\eta^{n+\frac{1}{2}}\mathbf{D}^{n+\frac{1}{2}}-p^{n+\frac{1}{2}}\mathbf{I}\right)\right]+\mathbf{b}^{n+\frac{1}{2}}\cdot\mathbf{v}^{n+\frac{1}{2}}\\&=-\left(\sigma_e^{n+\frac{1}{2}}+2\eta^{n+\frac{1}{2}}\mathbf{D}^{n+\frac{1}{2}}\right):\nabla\mathbf{v}^{n+\frac{1}{2}}+\nabla\cdot\left[\left(\sigma_e^{n+\frac{1}{2}}+2\eta^{n+\frac{1}{2}}\mathbf{D}^{n+\frac{1}{2}}\right.\right.\\&\quad\left.\left.-p^{n+\frac{1}{2}}\mathbf{I}\right)\cdot\mathbf{v}^{n+\frac{1}{2}}\right]+\mathbf{b}^{n+\frac{1}{2}}\cdot\mathbf{v}^{n+\frac{1}{2}}.\end{aligned} \tag{4.24}$$

Using the definition of E^n and (4.13-4), we have

$$\begin{aligned}\frac{E^{n+1}-E^n}{\Delta t}&=\int_\Omega\left[\frac{e^{n+1}-e^n}{\Delta t}+\frac{\rho}{2}\frac{|\mathbf{v}^{n+1}|^2-|\mathbf{v}^n|^2}{\Delta t}\right]d\mathbf{x}\\&=\int_\Omega\left[-\nabla\cdot\mathbf{q}^{n+\frac{1}{2}}-\nabla\right.\\&\quad\left.\cdot\left(\bar{e}^{n+\frac{1}{2}}\mathbf{v}^{n+\frac{1}{2}}\right)+\nabla\cdot\left[\left(\sigma_e^{n+\frac{1}{2}}+2\eta^{n+\frac{1}{2}}\mathbf{D}^{n+\frac{1}{2}}-p^{n+\frac{1}{2}}\mathbf{I}\right)\cdot\mathbf{v}^{n+\frac{1}{2}}\right]\right.\\&\quad\left.-\nabla\cdot\left[\left(\frac{\rho}{2}|\mathbf{v}^{n+\frac{1}{2}}|^2\right)\bar{\mathbf{v}}^{n+\frac{1}{2}}+\mathbf{b}^{n+\frac{1}{2}}\cdot\mathbf{v}^{n+\frac{1}{2}}\right]d\mathbf{x}\right.\\&=\int_\Omega\mathbf{b}^{n+\frac{1}{2}}\cdot\mathbf{v}^{n+\frac{1}{2}}d\mathbf{x},\end{aligned} \tag{4.25}$$

where boundary conditions $\mathbf{v}^n|_{\partial\Omega} = 0$ and $\mathbf{n}\cdot\mathbf{q}^{n+\frac{1}{2}}|_{\partial\Omega} = 0$ are used. Then, Scheme 1 preserves the total energy conservation if $\mathbf{b}^{n+\frac{1}{2}}$=0.

By definition, we have

$$\begin{aligned}\frac{V^{n+1}-V^n}{\Delta t} &= \int_\Omega \frac{\phi^{n+1}-\phi^n}{\Delta t}d\mathbf{x}\\ &= -\int_\Omega \nabla\cdot\mathbf{M}\nabla\left(\gamma_1\Delta\phi^{n+\frac{1}{2}} - 2q^{n+\frac{1}{2}}q_\phi^{n+\frac{1}{2}} - 2\gamma_2\phi^{n+\frac{1}{2}}\right)\\ &\quad + \nabla\cdot\left(\bar{\phi}^{n+\frac{1}{2}}\mathbf{v}^{n+\frac{1}{2}}\right)d\mathbf{x} = 0,\end{aligned} \tag{4.26}$$

where boundary conditions $\mathbf{v}^n|_{\partial\Omega} = 0$ and $\mathbf{n}\cdot\nabla\frac{\delta S}{\delta\phi}^n|_{\partial\Omega} = 0$ are used.

From (4.13-1) and (4.13-4), we have

$$\begin{aligned}&\frac{S^{n+1}-S^n}{\Delta t}\\ &= \int_\Omega\left[-\left(q^{n+1}+q^n\right)\frac{q^{n+1}-q^n}{\Delta t} - \gamma_2\left(\phi^{n+1}+\phi^n\right)\frac{\phi^{n+1}-\phi^n}{\Delta t}\right.\\ &\quad \left.-\gamma_3\left(e^{n+1}+e^n\right)\frac{e^{n+1}-e^n}{\Delta t} - \frac{\gamma_1}{2}\left(\nabla\phi^{n+1}+\nabla\phi^n\right)\frac{\nabla\phi^{n+1}-\nabla\phi^n}{\Delta t}\right]d\mathbf{x}\\ &= \int_\Omega\left[-2\delta_t\phi^{n+\frac{1}{2}}q^{n+\frac{1}{2}}\bar{q}_\phi^{n+\frac{1}{2}} + \delta_t\phi^{n+\frac{1}{2}}\left(\gamma_1\Delta\phi^{n+\frac{1}{2}}\right) - 2\gamma_2\phi^{n+\frac{1}{2}}\left(-\nabla\cdot\mathbf{M}\nabla\frac{\delta S}{\delta\phi}^{n+\frac{1}{2}}\right)\right.\\ &\quad \left.+2\gamma_2\phi^{n+\frac{1}{2}}\nabla\cdot\left(\bar{\phi}^{n+\frac{1}{2}}\mathbf{v}^{n+\frac{1}{2}}\right) - 2\delta_t e^{n+\frac{1}{2}}q^{n+\frac{1}{2}}\bar{q}_e^{n+\frac{1}{2}} - 2\gamma_3 e^{n+\frac{1}{2}}\delta_t e^{n+\frac{1}{2}}\right]d\mathbf{x}\\ &= \int_\Omega\left[\delta_t\phi^{n+\frac{1}{2}}\frac{\delta S}{\delta\phi}^{n+\frac{1}{2}} - 2\gamma_2\phi^{n+\frac{1}{2}}\left(-\nabla\cdot\mathbf{M}\nabla\frac{\delta S}{\delta\phi}^{n+\frac{1}{2}} - \delta_t\phi^{n+\frac{1}{2}}\right)\right.\\ &\quad \left.+2\gamma_2\phi^{n+\frac{1}{2}}\nabla\cdot\left(\bar{\phi}^{n+\frac{1}{2}}\mathbf{v}^{n+\frac{1}{2}}\right) + \delta_t e^{n+\frac{1}{2}}\frac{\delta S}{\delta e}^{n+\frac{1}{2}}\right]d\mathbf{x}\\ &= \int_\Omega\left(\delta_t\phi^{n+\frac{1}{2}}\frac{\delta S}{\delta\phi}^{n+\frac{1}{2}} + \delta_t e^{n+\frac{1}{2}}\frac{\delta S}{\delta e}^{n+\frac{1}{2}}\right)d\mathbf{x}.\end{aligned} \tag{4.27}$$

Multiplying $\delta_t\phi^{n+\frac{1}{2}}$ by $\frac{\delta S}{\delta\phi}^{n+\frac{1}{2}}$, $\delta_t e^{n+\frac{1}{2}}$ by $\frac{\delta S}{\delta e}^{n+\frac{1}{2}}$, adding them up and integrating them in space, we have

$$\begin{aligned}&\int_\Omega\left(\delta_t\phi^{n+\frac{1}{2}}\frac{\delta S}{\delta\phi}^{n+\frac{1}{2}} + \delta_t e^{n+\frac{1}{2}}\frac{\delta S}{\delta e}^{n+\frac{1}{2}}\right)d\mathbf{x}\\ &= \int_\Omega\left[\left(-\nabla\cdot\mathbf{M}\nabla\frac{\delta S}{\delta\phi}^{n+\frac{1}{2}} - \nabla\cdot\left(\bar{\phi}^{n+\frac{1}{2}}\mathbf{v}^{n+\frac{1}{2}}\right)\right)\frac{\delta S}{\delta\phi}^{n+\frac{1}{2}}\right.\\ &\quad \left.+\left(\left(\sigma_e^{n+\frac{1}{2}} + 2\eta^{n+\frac{1}{2}}\mathbf{D}^{n+\frac{1}{2}}\right):\nabla\mathbf{v}^{n+\frac{1}{2}} - \nabla\cdot\left(\bar{D}_e^{n+\frac{1}{2}}\nabla\frac{\delta S}{\delta e}^{n+\frac{1}{2}}\right) - \nabla\cdot\left(\bar{e}^{n+\frac{1}{2}}\mathbf{v}^{n+\frac{1}{2}}\right)\right)\frac{\delta S}{\delta e}^{n+\frac{1}{2}}\right]d\mathbf{x}\end{aligned}$$

$$
\begin{aligned}
&= \int_\Omega \mathbf{M}\left(\nabla \frac{\delta S}{\delta \phi}^{n+\frac{1}{2}}\right)^2 + 2\eta^{n+\frac{1}{2}} \frac{\delta S}{\delta e}^{n+\frac{1}{2}} \mathbf{D}^{n+\frac{1}{2}} : \nabla \mathbf{v}^{n+\frac{1}{2}} + \bar{D}_e^{n+\frac{1}{2}} \left(\nabla \frac{\delta S}{\delta e}^{n+\frac{1}{2}}\right)^2 \\
&\quad + \frac{\delta S}{\delta e}^{n+\frac{1}{2}} \sigma_e^{n+\frac{1}{2}} : \nabla \mathbf{v}^{n+\frac{1}{2}} + \left(s_*^{n+\frac{1}{2}} \mathbf{I} - \frac{\partial s}{\partial \nabla \phi}^{n+\frac{1}{2}} \nabla \phi^{n+\frac{1}{2}}\right) : \nabla \mathbf{v}^{n+\frac{1}{2}} d\mathbf{x} \\
&\quad - \int_{\partial\Omega} \mathbf{n} \cdot \left(s_*^{n+\frac{1}{2}} \mathbf{I} - \frac{\partial s}{\partial \nabla \phi}^{n+\frac{1}{2}} \nabla \phi^{n+\frac{1}{2}}\right) \cdot \mathbf{v}^{n+\frac{1}{2}} d\mathbf{a} - \int_{\partial\Omega} \mathbf{n} \cdot \left(\frac{\delta S}{\delta e}^{n+\frac{1}{2}} \bar{D}_e^{n+\frac{1}{2}} \nabla \frac{\delta S}{\delta e}^{n+\frac{1}{2}}\right) d\mathbf{a} \\
&= \int_\Omega \left[\mathbf{M}\left(\nabla \frac{\delta S}{\delta \phi}^{n+\frac{1}{2}}\right)^2 + 2\eta^{n+\frac{1}{2}} \left(\frac{1}{T}\right)^{n+\frac{1}{2}} \mathbf{D}^{n+\frac{1}{2}} : \mathbf{D}^{n+\frac{1}{2}} \right. \\
&\quad \left. + \bar{D}_e^{n+\frac{1}{2}} \left|\nabla \frac{\delta S}{\delta e}^{n+\frac{1}{2}}\right|^2\right] d\mathbf{x} - \int_{\partial\Omega} \mathbf{n} \cdot \left(\frac{\delta S}{\delta e}^{n+\frac{1}{2}} \bar{D}_e^{n+\frac{1}{2}} \nabla \frac{\delta S}{\delta e}^{n+\frac{1}{2}}\right) d\mathbf{a}, \qquad (4.28)
\end{aligned}
$$

where we use $\mathbf{I} : \nabla \mathbf{v}^{n+\frac{1}{2}} = 0$ and assume there exists a function s_* such that

$$
\nabla s_*^{n+\frac{1}{2}} = \frac{\delta S}{\delta \phi}^{n+\frac{1}{2}} \nabla \bar{\phi}^{n+\frac{1}{2}} + \frac{\delta S}{\delta e}^{n+\frac{1}{2}} \nabla \bar{e}^{n+\frac{1}{2}} + \nabla \cdot \left(\frac{\partial s}{\partial \nabla \phi}^{n+\frac{1}{2}} \nabla \phi^{n+\frac{1}{2}}\right). \qquad (4.29)
$$

The existence of s_* is warranted by the solution of the Poisson equation subject to Neumann boundary conditions. From the above result, we conclude that Scheme 1 preserves the positive entropy production rate

$$
\begin{aligned}
&\frac{S^{n+1} - S^n}{\Delta t}|_{gen} \\
&= \int_\Omega \left[\mathbf{M}\left(\nabla \frac{\delta S}{\delta \phi}^{n+\frac{1}{2}}\right)^2 + 2\eta^{n+\frac{1}{2}} \left(\frac{1}{T}\right)^{n+\frac{1}{2}} \mathbf{D}^{n+\frac{1}{2}} : \mathbf{D}^{n+\frac{1}{2}} + \bar{D}_e^{n+\frac{1}{2}} \left|\nabla \frac{\delta S}{\delta e}^{n+\frac{1}{2}}\right|^2\right] \\
&\quad d\mathbf{x} \geq 0. \qquad (4.30)
\end{aligned}
$$

□

4.3 Spatial Discretization

Here, we apply the finite difference on staggered-grids in space to semi-discrete Scheme 1 to arrive at a fully discrete (Scheme 2) and then show the fully discrete scheme preserves energy, mass and the entropy production rate as well.

Scheme 2 **(Fully discrete EQ Scheme)**

$$
\begin{cases}
\left\{\delta_t\phi^{n+\frac{1}{2}} + d_x\left(A_x\bar{\phi}^{n+\frac{1}{2}}u^{n+\frac{1}{2}}\right) + d_y\left(A_y\bar{\phi}^{n+\frac{1}{2}}v^{n+\frac{1}{2}}\right)\right.\\
\left. = -\nabla_h\cdot\mathbf{M}\nabla_h\left(\gamma_1\Delta_h\phi^{n+\frac{1}{2}} - 2q^{n+\frac{1}{2}}\bar{q}_\phi^{n+\frac{1}{2}} - 2\gamma_2\phi^{n+\frac{1}{2}}\right)\right\}|_{i,j}, i=1,2,\ldots,N_x,\ j=1,2,\ldots,N_y.\\

\left\{\delta_t e^{n+\frac{1}{2}} + d_x\left(A_x\bar{e}^{n+\frac{1}{2}}u^{n+\frac{1}{2}}\right) + d_y\left(A_y\bar{e}^{n+\frac{1}{2}}v^{n+\frac{1}{2}}\right)\right.\\
= \left(-T^{n+\frac{1}{2}}\gamma_1\right)\left[d_x\left(A_x\phi^{n+\frac{1}{2}}\right)^2 d_x u^{n+\frac{1}{2}} + d_x\left(A_x\phi^{n+\frac{1}{2}}\right)d_y\left(A_y\phi^{n+\frac{1}{2}}\right)\right.\\
\left.\left(a_y D_y a_x u^{n+\frac{1}{2}} + a_x D_x a_y v^{n+\frac{1}{2}}\right) + d_y\left(A_y\phi^{n+\frac{1}{2}}\right)^2 d_y v^{n+\frac{1}{2}}\right]\\
\quad +2\eta\left[\left(d_x u^{n+\frac{1}{2}}\right)^2 + \frac{1}{2}\left(a_x D_x a_y v^{n+\frac{1}{2}} + a_y D_y a_x u^{n+\frac{1}{2}}\right)^2 + \left(d_y v^{n+\frac{1}{2}}\right)^2\right]\\
\quad -\nabla_h\cdot\left(\bar{D_e}^{n+\frac{1}{2}}\nabla_h\left(\frac{1}{T}\right)^{n+\frac{1}{2}}\right)\Big\}|_{i,j}, i=1,2,\ldots,N_x,\ j=1,2,\ldots,N_y.\\

\left\{\delta_t q^{n+\frac{1}{2}} = \bar{q}_\phi^{n+\frac{1}{2}}\delta_t\phi^{n+\frac{1}{2}} + \bar{q}_e^{n+\frac{1}{2}}\delta_t e^{n+\frac{1}{2}}\right\}|_{i,j}, i=1,2,\ldots,N_x,\ j=1,2,\ldots,N_y.\\

\left\{d_x u^{n+\frac{1}{2}} + d_y v^{n+\frac{1}{2}} = 0\right\}|_{i,j}, i=1,2,\ldots,N_x,\ j=1,2,\ldots,N_y.\\

\left\{\rho\left[\delta_t u^{n+\frac{1}{2}} + \frac{1}{2}\left(\bar{u}^{n+\frac{1}{2}}D_x\left(a_x u^{n+\frac{1}{2}}\right) + A_x\left(d_x\left(u^{n+\frac{1}{2}}\bar{u}^{n+\frac{1}{2}}\right)\right)\right.\right.\right.\\
\left.\left.\left. + a_y\left(A_x\bar{v}^{n+\frac{1}{2}}D_y u^{n+\frac{1}{2}}\right) + d_y\left(A_y u^{n+\frac{1}{2}}A_x\bar{v}^{n+\frac{1}{2}}\right)\right)\right]\right.\\
= -D_x p^{n+\frac{1}{2}} + \left[d_x A_x\left(\left(-T^{n+\frac{1}{2}}\gamma_1\right)\left(d_x\phi^{n+\frac{1}{2}}\right)^2\right)\right.\\
\left.+ d_y A_y\left(\left(-T^{n+\frac{1}{2}}\gamma_1\right)\left(d_x\phi^{n+\frac{1}{2}}\right)\left(a_y D_y a_x\phi^{n+\frac{1}{2}}\right)\right)\right]\\
+\eta^{n+\frac{1}{2}}\Delta_h u^{n+\frac{1}{2}} + 2D_x\eta^{n+\frac{1}{2}}\\
\left.D_x\left(a_x u^{n+\frac{1}{2}}\right) + A_x D_y\eta^{n+\frac{1}{2}}\left(D_y u^{n+\frac{1}{2}} + A_y d_x v^{n+\frac{1}{2}}\right) + b_1^{n+\frac{1}{2}}\right\}|_{i+\frac{1}{2},j},\\
i=1,2,\ldots,N_x-1,\ j=1,2,\ldots,N_y.\\

\{\rho\left[\delta_t v^{n+\frac{1}{2}} + \frac{1}{2}\left(a_x\left(A_y\bar{u}^{n+\frac{1}{2}}D_x v^{n+\frac{1}{2}}\right) + d_x\left(A_y\bar{u}^{n+\frac{1}{2}}A_x v^{n+\frac{1}{2}}\right)\right.\right.\\
\left.\left. + \bar{v}^{n+\frac{1}{2}}D_y\left(a_y v^{n+\frac{1}{2}}\right) + A_y\left(d_y\left(v^{n+\frac{1}{2}}\bar{v}^{n+\frac{1}{2}}\right)\right)\right)\right]\\
= -D_y p^{n+\frac{1}{2}} + \left[d_y A_y\left(\left(-T^{n+\frac{1}{2}}\gamma_1\right)\left(d_y\phi^{n+\frac{1}{2}}\right)^2\right)\right.\\
\left.+ d_x A_x\left(\left(-T^{n+\frac{1}{2}}\gamma_1\right)\left(d_y\phi^{n+\frac{1}{2}}\right)\left(a_x D_x a_y\phi^{n+\frac{1}{2}}\right)\right)\right]\\
+\eta^{n+\frac{1}{2}}\Delta_h v^{n+\frac{1}{2}} + 2D_y\eta^{n+\frac{1}{2}}D_y\left(a_y v^{n+\frac{1}{2}}\right) + A_y D_x\eta^{n+\frac{1}{2}}\left(D_x v^{n+\frac{1}{2}} + A_x d_y u^{n+\frac{1}{2}}\right) + b_2^{n+\frac{1}{2}}\}|_{i,j+\frac{1}{2}},\\
i=1,2,\ldots,N_x,\ j=1,2,\ldots,N_y-1,
\end{cases}
\tag{4.31}
$$

where

$$
T^{n+\frac{1}{2}} = \frac{\delta e}{\delta S}^{n+\frac{1}{2}} = -\frac{1}{2(q^{n+\frac{1}{2}}\bar{q_e}^{n+\frac{1}{2}} + \gamma_3 e^{n+\frac{1}{2}})},
$$

$$\eta^{n+\frac{1}{2}} = A_0 e^{\left(\frac{B_0}{T}\right)^{n+\frac{1}{2}}} = A_0 e^{-2B_0\left(q^{n+\frac{1}{2}}\bar{q}_e^{n+\frac{1}{2}}+\gamma_3 e^{n+\frac{1}{2}}\right)}. \tag{4.32}$$

The physical boundary conditions are discretized as follows

$$u^n, D_x\phi^n, D_x\frac{\delta s}{\delta\phi}^n, D_x e^n \in \varepsilon^{ew0}_{x\times y}, \quad v^n, D_y\phi^n, D_y\frac{\delta s}{\delta\phi}^n, D_y e^n \in \varepsilon^{ns0}_{x\times y}. \tag{4.33}$$

Theorem 4.2 *1. Under boundary conditions (4.33), Scheme 2 preserves the total energy balance*

$$E_h^{n+1} - E_h^n = \left[b_1^{n+\frac{1}{2}}, u^{n+\frac{1}{2}}\right]_{ew} + \left[b_2^{n+\frac{1}{2}}, v^{n+\frac{1}{2}}\right]_{ns}, \tag{4.34}$$

where

$$E_h^n = (e^n, 1)_2 + \frac{\rho}{2}\|\mathbf{v}^n\|_2^2. \tag{4.35}$$

If $\mathbf{b}^{n+\frac{1}{2}}$*=0,* $E_h^{n+1} = E_h^n$*, i.e., Scheme 2 conserves the total energy conservation.*

2. Scheme 2 preserves the volume of fluid A:

$$V_h^{n+1} = V_h^n, \tag{4.36}$$

where

$$V_h^n = (\phi^n, 1)_2. \tag{4.37}$$

3. Scheme 2 preserves the positive entropy production rate,

$$\begin{aligned}
&\frac{S_h^{n+1} - S_h^n}{\Delta t}|_{gen} \\
&= \left(\left(\frac{1}{T}\right)^{n+\frac{1}{2}}, 2\eta^{n+\frac{1}{2}}\left[\left(d_x u^{n+\frac{1}{2}}\right)^2 + \frac{1}{2}\left(a_x D_x a_y v^{n+\frac{1}{2}} + a_y D_y a_x u^{n+\frac{1}{2}}\right)^2\right.\right. \\
&\left.\left. + \left(d_y v^{n+\frac{1}{2}}\right)^2\right]\right)_2 \\
&+ \left(\mathbf{M}\nabla_h\frac{\delta S}{\delta\phi}^{n+\frac{1}{2}}, \nabla_h\frac{\delta S}{\delta\phi}^{n+\frac{1}{2}}\right)_2 \\
&+ D_0\sum_{i=1}^{N_x-1}\sum_{j=1}^{N_y-1}\left(\frac{\left(T_{i+1,j}^{n+\frac{1}{2}} - T_{i,j}^{n+\frac{1}{2}}\right)^2}{T_{i,j}^{n+\frac{1}{2}}T_{i+1,j}^{n+\frac{1}{2}}} + \frac{\left(T_{i,j+1}^{n+\frac{1}{2}} - T_{i,j}^{n+\frac{1}{2}}\right)^2}{T_{i,j}^{n+\frac{1}{2}}T_{i,j+1}^{n+\frac{1}{2}}}\right) \geq 0,
\end{aligned} \tag{4.38}$$

where

$$S_h^n = -\|q^n\|_2^2 - \gamma_2\|\phi^n\|_2^2 - \gamma_3\|e^n\|_2^2 - \frac{\gamma_1}{2}\|\nabla_h\phi^n\|_2^2 + (C_0, 1)_2. \tag{4.39}$$

Proof We denote

$$\begin{aligned}
\frac{\delta S}{\delta\phi}^{n+\frac{1}{2}} &= \gamma_1\Delta_h\phi^{n+\frac{1}{2}} - 2q^{n+\frac{1}{2}}\bar{q}_\phi^{n+\frac{1}{2}} - 2\gamma_2\phi^{n+\frac{1}{2}}, \\
\frac{\delta S}{\delta e}^{n+\frac{1}{2}} &= -2q^{n+\frac{1}{2}}\bar{q}_e^{n+\frac{1}{2}} - 2\gamma_3 e^{n+\frac{1}{2}} = \left(\frac{1}{T}\right)^{n+\frac{1}{2}}.
\end{aligned} \tag{4.40}$$

Noticing the fully discrete physical boundary conditions are given by conditions (3.5), (3.6), we have

$$\begin{aligned}\frac{S_h^{n+1}-S_h^n}{\Delta t} &= -\left(q^{n+1}+q^n, \frac{q^{n+1}-q^n}{\Delta t}\right)_2 - \gamma_2\left(\phi^{n+1}+\phi^n, \frac{\phi^{n+1}-\phi^n}{\Delta t}\right)_2 \\ &\quad -\gamma_3\left(e^{n+1}+e^n, \frac{e^{n+1}-e^n}{\Delta t}\right)_2 - \frac{\gamma_1}{2}\left(\left[D_x\phi^{n+\frac{1}{2}}, D_x\delta_t\phi^{n+\frac{1}{2}}\right]_{ew}\right. \\ &\quad \left.+\left[D_y\phi^{n+\frac{1}{2}}, D_y\delta_t\phi^{n+\frac{1}{2}}\right]_{ns}\right) \\ &= \left(\delta_t\phi^{n+\frac{1}{2}}, \frac{\delta S}{\delta\phi}^{n+\frac{1}{2}}\right)_2 + \left(\delta_t e^{n+\frac{1}{2}}, \frac{\delta S}{\delta e}^{n+\frac{1}{2}}\right)_2, \end{aligned} \tag{4.41}$$

Applying (4.31-1) and (4.31-2), we have

$$\begin{aligned}\left(\delta_t\phi^{n+\frac{1}{2}}, \frac{\delta S}{\delta\phi}^{n+\frac{1}{2}}\right)_2 &= \left(\mathbf{M}\nabla_h\frac{\delta S}{\delta\phi}^{n+\frac{1}{2}}, \nabla_h\frac{\delta S}{\delta\phi}^{n+\frac{1}{2}}\right)_2 \\ &\quad -\left(d_x\left(A_x\bar{\phi}^{n+\frac{1}{2}}u^{n+\frac{1}{2}}\right)+d_y\left(A_y\bar{\phi}^{n+\frac{1}{2}}v^{n+\frac{1}{2}}\right), \frac{\delta S}{\delta\phi}^{n+\frac{1}{2}}\right)_2, \end{aligned} \tag{4.42}$$

and

$$\begin{aligned}&\left(\delta_t e^{n+\frac{1}{2}}, \frac{\delta S}{\delta e}^{n+\frac{1}{2}}\right)_2 \\ &= \left(\left(\frac{1}{T}\right)^{n+\frac{1}{2}}, \left(-T^{n+\frac{1}{2}}\gamma_1\right)\left[d_x\left(A_x\phi^{n+\frac{1}{2}}\right)d_x\left(A_x\bar{\phi}^{n+\frac{1}{2}}\right)d_x u^{n+\frac{1}{2}}\right.\right. \\ &\quad + d_x\left(A_x\phi^{n+\frac{1}{2}}\right)d_y\left(A_y\bar{\phi}^{n+\frac{1}{2}}\right)a_y D_y a_x u^{n+\frac{1}{2}} \\ &\quad \left.\left. + d_x\left(A_x\bar{\phi}^{n+\frac{1}{2}}\right)d_y\left(A_y\phi^{n+\frac{1}{2}}\right)a_x D_x a_y v^{n+\frac{1}{2}} + d_y\left(A_y\bar{\phi}^{n+\frac{1}{2}}\right)d_y\left(A_y\phi^{n+\frac{1}{2}}\right)d_y v^{n+\frac{1}{2}}\right]\right)_2 \\ &\quad + \left(\left(\frac{1}{T}\right)^{n+\frac{1}{2}}, 2\eta^{n+\frac{1}{2}}\left[\left(d_x u^{n+\frac{1}{2}}\right)^2 + \frac{1}{2}\left(a_x D_x a_y v^{n+\frac{1}{2}} + a_y D_y a_x u^{n+\frac{1}{2}}\right)^2 + \left(d_y v^{n+\frac{1}{2}}\right)^2\right]\right)_2 \\ &\quad + \left(\left(\frac{1}{T}\right)^{n+\frac{1}{2}}, D_0\Delta_h T^{n+\frac{1}{2}}\right)_2 - \left(d_x\left(A_x\bar{e}^{n+\frac{1}{2}}u^{n+\frac{1}{2}}\right)+d_y\left(A_y\bar{e}^{n+\frac{1}{2}}v^{n+\frac{1}{2}}\right), \frac{\delta S}{\delta e}^{n+\frac{1}{2}}\right)_2. \end{aligned} \tag{4.43}$$

We calculate

$$\begin{aligned}&\left(d_x\left(A_x\bar{\phi}^{n+\frac{1}{2}}u^{n+\frac{1}{2}}\right)+d_y\left(A_y\bar{\phi}^{n+\frac{1}{2}}v^{n+\frac{1}{2}}\right), \frac{\delta S}{\delta\phi}^{n+\frac{1}{2}}\right)_2 \\ &\quad + \left(d_x\left(A_x\bar{e}^{n+\frac{1}{2}}u^{n+\frac{1}{2}}\right)+d_y\left(A_y\bar{e}^{n+\frac{1}{2}}v^{n+\frac{1}{2}}\right), \frac{\delta S}{\delta e}^{n+\frac{1}{2}}\right)_2 \\ &= \left(a_x\left(D_x\bar{\phi}^{n+\frac{1}{2}}u^{n+\frac{1}{2}}\right)+a_y\left(D_y\bar{\phi}^{n+\frac{1}{2}}v^{n+\frac{1}{2}}\right), \frac{\delta S}{\delta\phi}^{n+\frac{1}{2}}\right)_2 \\ &\quad + \left(a_x\left(D_x\bar{e}^{n+\frac{1}{2}}u^{n+\frac{1}{2}}\right)+a_y\left(D_y\bar{e}^{n+\frac{1}{2}}v^{n+\frac{1}{2}}\right), \frac{\delta S}{\delta e}^{n+\frac{1}{2}}\right)_2 \end{aligned}$$

$$= \left[A_x \frac{\delta S^{n+\frac{1}{2}}}{\delta \phi} D_x \bar{\phi}^{n+\frac{1}{2}} + A_x \frac{\delta S^{n+\frac{1}{2}}}{\delta e} D_x \bar{e}^{n+\frac{1}{2}}, u^{n+\frac{1}{2}} \right]_{ew} + \left[A_y \frac{\delta S^{n+\frac{1}{2}}}{\delta \phi} D_y \bar{\phi}^{n+\frac{1}{2}} + A_y \frac{\delta S^{n+\frac{1}{2}}}{\delta e} D_y \bar{e}^{n+\frac{1}{2}}, v^{n+\frac{1}{2}} \right]_{ns}, \tag{4.44}$$

where the following equalities are used

$$\begin{aligned}
&d_x(A_x\phi u) = \phi d_x u + a_x(D_x\phi u), \quad d_y(A_y\phi v) = \phi d_y v + a_y(D_y\phi v),\\
&d_x(A_x e u) = e d_x u + a_x(D_x e u), \quad d_y(A_y e v) = e d_y v + a_y(D_y e v), \quad d_x u + d_y v = 0,\\
&\left(a_x(D_x\phi u), \frac{\delta S}{\delta \phi}\right)_2 = \left[A_x \frac{\delta S}{\delta \phi} D_x\phi, u\right]_{ew}, \quad \left(a_y(D_y\phi v), \frac{\delta S}{\delta \phi}\right)_2 = \left[A_y \frac{\delta S}{\delta \phi} D_y\phi, v\right]_{ns},\\
&\left(a_x(D_x e u), \frac{\delta S}{\delta e}\right)_2 = \left[A_x \frac{\delta S}{\delta e} D_x e, u\right]_{ew}, \quad \left(a_y(D_y e v), \frac{\delta S}{\delta e}\right)_2 = \left[A_y \frac{\delta S}{\delta e} D_y e, v\right]_{ns}.
\end{aligned} \tag{4.45}$$

Meanwhile, under condition (4.29), we have

$$\begin{aligned}
D_x s_*^{n+\frac{1}{2}} &= A_x \frac{\delta S^{n+\frac{1}{2}}}{\delta \phi} D_x \bar{\phi}^{n+\frac{1}{2}} + A_x \frac{\delta S^{n+\frac{1}{2}}}{\delta e} D_x \bar{e}^{n+\frac{1}{2}}\\
&\quad -\gamma_1 \left[D_x \left(d_x \left(A_x \phi^{n+\frac{1}{2}} \right) d_x \left(A_x \bar{\phi}^{n+\frac{1}{2}} \right) \right) \right.\\
&\quad \left. + D_y a_x a_y \left(d_x \left(A_x \bar{\phi}^{n+\frac{1}{2}} \right) d_y \left(A_y \phi^{n+\frac{1}{2}} \right) \right) \right],\\
D_y s_*^{n+\frac{1}{2}} &= A_y \frac{\delta S^{n+\frac{1}{2}}}{\delta \phi} D_y \bar{\phi}^{n+\frac{1}{2}} + A_y \frac{\delta S^{n+\frac{1}{2}}}{\delta e} D_y \bar{e}^{n+\frac{1}{2}}\\
&\quad -\gamma_1 \left[D_y \left(d_y \left(A_y \bar{\phi}^{n+\frac{1}{2}} \right) d_y \left(A_y \phi^{n+\frac{1}{2}} \right) \right) \right.\\
&\quad \left. + D_x a_y a_x \left(d_x \left(A_x \phi^{n+\frac{1}{2}} \right) d_y \left(A_y \bar{\phi}^{n+\frac{1}{2}} \right) \right) \right].
\end{aligned} \tag{4.46}$$

Then, we arrive at

$$\begin{aligned}
&\left[A_x \frac{\delta S^{n+\frac{1}{2}}}{\delta \phi} D_x \bar{\phi}^{n+\frac{1}{2}} + A_x \frac{\delta S^{n+\frac{1}{2}}}{\delta e} D_x \bar{e}^{n+\frac{1}{2}}, u^{n+\frac{1}{2}} \right]_{ew}\\
&\quad + \left[A_y \frac{\delta S^{n+\frac{1}{2}}}{\delta \phi} D_y \bar{\phi}^{n+\frac{1}{2}} + A_y \frac{\delta S^{n+\frac{1}{2}}}{\delta e} D_y \bar{e}^{n+\frac{1}{2}}, v^{n+\frac{1}{2}} \right]_{ns}\\
&= -\gamma_1 \left[\left(d_x \left(A_x \phi^{n+\frac{1}{2}} \right) d_x \left(A_x \bar{\phi}^{n+\frac{1}{2}} \right), d_x u^{n+\frac{1}{2}} \right)_2 \right.\\
&\quad + \left(d_y \left(A_y \phi^{n+\frac{1}{2}} \right) d_y \left(A_y \bar{\phi}^{n+\frac{1}{2}} \right), d_y v^{n+\frac{1}{2}} \right)_2\\
&\quad + \left(d_x \left(A_x \bar{\phi}^{n+\frac{1}{2}} \right) d_y \left(A_y \phi^{n+\frac{1}{2}} \right), a_y D_y a_x u^{n+\frac{1}{2}} \right)_2\\
&\quad \left. + \left(d_x \left(A_x \phi^{n+\frac{1}{2}} \right) d_y \left(A_y \bar{\phi}^{n+\frac{1}{2}} \right), a_x D_x a_y v^{n+\frac{1}{2}} \right)_2 \right],
\end{aligned} \tag{4.47}$$

where we use the equalities

$$\begin{aligned}
&[D_x s_*, u]_{ew} = -(s_*, d_x u)_2, \quad [D_y s_*, v]_{ns} = -(s_*, d_y v)_2, \quad d_x u + d_y v = 0\\
&[D_y a_x a_y \phi, u]_{ew} = -(\phi, a_y D_y a_x u)_2, \quad [D_x a_y a_x \phi, v]_{ns} = -(\phi, a_x D_x a_y v)_2.
\end{aligned} \tag{4.48}$$

From the above results, we obtain

$$\begin{aligned}
&\left(\delta_t \phi^{n+\frac{1}{2}}, \frac{\delta S}{\delta \phi}^{n+\frac{1}{2}}\right)_2 + \left(\delta_t e^{n+\frac{1}{2}}, \frac{\delta S}{\delta e}^{n+\frac{1}{2}}\right)_2 \\
&= \left(\mathbf{M}\nabla_h \frac{\delta S}{\delta \phi}^{n+\frac{1}{2}}, \nabla_h \frac{\delta S}{\delta \phi}^{n+\frac{1}{2}}\right)_2 + \left(\left(\frac{1}{T}\right)^{n+\frac{1}{2}}, 2\eta^{n+\frac{1}{2}}\left[\left(d_x u^{n+\frac{1}{2}}\right)^2\right.\right. \\
&\quad \left.\left. + \frac{1}{2}\left(a_x D_x a_y v^{n+\frac{1}{2}} + a_y D_y a_x u^{n+\frac{1}{2}}\right)^2 + \left(d_y v^{n+\frac{1}{2}}\right)^2\right]\right)_2 + \left(\left(\frac{1}{T}\right)^{n+\frac{1}{2}}, D_0 \Delta_h T^{n+\frac{1}{2}}\right)_2.
\end{aligned} \tag{4.49}$$

With Neumann boundary conditions (2.16) $\mathbf{n}\cdot\mathbf{q}^{n+\frac{1}{2}} \neq 0$, we have

$$\begin{aligned}
&\left(\left(\frac{1}{T}\right)^{n+\frac{1}{2}}, D_0 \Delta_h T^{n+\frac{1}{2}}\right)_2 \\
&= D_0 \sum_{i=1}^{N_x-1}\sum_{j=1}^{N_y-1}\left(\frac{\left(T_{i+1,j}^{n+\frac{1}{2}} - T_{i,j}^{n+\frac{1}{2}}\right)^2}{T_{i,j}^{n+\frac{1}{2}} T_{i+1,j}^{n+\frac{1}{2}}} + \frac{\left(T_{i,j+1}^{n+\frac{1}{2}} - T_{i,j}^{n+\frac{1}{2}}\right)^2}{T_{i,j}^{n+\frac{1}{2}} T_{i,j+1}^{n+\frac{1}{2}}}\right) \\
&\quad + D_0 h\left[\sum_{j=1}^{N_y}\left(\delta_x T_{N_x+1/2,j}^{n+\frac{1}{2}}\left(\frac{1}{T}\right)_{N_x,j}^{n+\frac{1}{2}} - \delta_x T_{N_1/2,j}^{n+\frac{1}{2}}\left(\frac{1}{T}\right)_{1,j}^{n+\frac{1}{2}}\right)\right. \\
&\quad \left. + \sum_{i=1}^{N_x}\left(\delta_y T_{i,N_y+1/2}^{n+\frac{1}{2}}\left(\frac{1}{T}\right)_{i,N_y}^{n+\frac{1}{2}} - \delta_y T_{i,1/2}^{n+\frac{1}{2}}\left(\frac{1}{T}\right)_{i,1}^{n+\frac{1}{2}}\right)\right].
\end{aligned} \tag{4.50}$$

Finally, we show that the fully discrete scheme 2 preserves the positive entropy production rate

$$\begin{aligned}
\frac{S_h^{n+1} - S_h^n}{\Delta t}|_{gen} &= \left(\left(\frac{1}{T}\right)^{n+\frac{1}{2}}, 2\eta^{n+\frac{1}{2}}\left[\left(d_x u^{n+\frac{1}{2}}\right)^2 + \frac{1}{2}\left(a_x D_x a_y v^{n+\frac{1}{2}} + a_y D_y a_x u^{n+\frac{1}{2}}\right)^2\right.\right. \\
&\quad \left.\left. + \left(d_y v^{n+\frac{1}{2}}\right)^2\right]\right)_2 + \left(\mathbf{M}\nabla_h \frac{\delta S}{\delta \phi}^{n+\frac{1}{2}}, \nabla_h \frac{\delta S}{\delta \phi}^{n+\frac{1}{2}}\right)_2 \\
&\quad + D_0 \sum_{i=1}^{N_x-1}\sum_{j=1}^{N_y-1}\left(\frac{\left(T_{i+1,j}^{n+\frac{1}{2}} - T_{i,j}^{n+\frac{1}{2}}\right)^2}{T_{i,j}^{n+\frac{1}{2}} T_{i+1,j}^{n+\frac{1}{2}}} + \frac{\left(T_{i,j+1}^{n+\frac{1}{2}} - T_{i,j}^{n+\frac{1}{2}}\right)^2}{T_{i,j}^{n+\frac{1}{2}} T_{i,j+1}^{n+\frac{1}{2}}}\right) \geq 0.
\end{aligned} \tag{4.51}$$

Computing the discrete inner product of (4.31-1) with constant function 1, and using (4.33) and Lemma 3.2, we obtain $\frac{V_h^{n+1} - V_h^n}{\Delta t} = 0$, i.e., Scheme 2 preserves the volume conservation. Meanwhile, combining the discrete inner product of (4.31-2) with constant function 1, (4.31-5) with constant function $u^{n+\frac{1}{2}}$ and (4.31-6) with constant function $v^{n+\frac{1}{2}}$, and applying (4.33)

and Lemmas 3.2–3.4 to it, we get

$$\frac{E_h^{n+1}-E_h^n}{\Delta t}=\left(\frac{e^{n+1}-e^n}{\Delta t},1\right)_2+\frac{\rho}{2}\left(\left[u^{n+\frac{1}{2}},\frac{u^{n+1}-u^n}{\Delta t}\right]_{ew}+\left[v^{n+\frac{1}{2}},\frac{v^{n+1}-v^n}{\Delta t}\right]_{ns}\right)$$
$$=\left[b_1^{n+\frac{1}{2}},u^{n+\frac{1}{2}}\right]_{ew}+\left[b_2^{n+\frac{1}{2}},v^{n+\frac{1}{2}}\right]_{ns}. \tag{4.52}$$

If $\mathbf{b}^{n+\frac{1}{2}}=0$, so $E_h^{n+1}=E_h^n$, i.e., Scheme 2 preserves the total energy conservation. □

4.4 Implementation of the Fully Discrete Scheme

In Scheme 2, there are nonlinear terms and variable coefficients in the resulting discrete equation system. A linearization is needed for efficient solution procedures at each time step. This is accomplished by adopting an iterative algorithm, in which a fast algorithm is employed to speed up the computation of the equations. The iterative algorithm is given as follows.

Scheme 3 **(Implementation of the EQ scheme)** For $n=0,1,2,3,\cdots,N$, we do the following.

1. Assign $\phi^{n+\frac{1}{2}(k=0)}=\phi^n$, $\mathbf{v}^{n+\frac{1}{2}(k=0)}=\mathbf{v}^n$, $e^{n+\frac{1}{2}(k=0)}=e^n$ initially.
2. Apply a fast Fourier algorithm to solve $\phi^{n+\frac{1}{2}(k+1)}$ from

$$\left(\frac{2}{\Delta t}+\mathbf{M}\gamma_1\Delta_h^2-2\mathbf{M}\gamma_2\Delta_h\right)\phi^{n+\frac{1}{2}(k+1)}$$
$$=\frac{2}{\Delta t}\phi^n+2\mathbf{M}\Delta_h\left[q^n\bar{q}_\phi^{n+\frac{1}{2}}+\left(\bar{q}_\phi^{n+\frac{1}{2}}\right)^2\left(\phi^{n+\frac{1}{2}(k)}-\phi^n\right)\right]$$
$$+2\mathbf{M}\Delta_h\left[\bar{q}_e^{n+\frac{1}{2}}\bar{q}_\phi^{n+\frac{1}{2}}\left(e^{n+\frac{1}{2}(k)}-e^n\right)\right]$$
$$-\left[d_x\left(A_x\bar{\phi}^{n+\frac{1}{2}}u^{n+\frac{1}{2}(k)}\right)+d_y\left(A_y\bar{\phi}^{n+\frac{1}{2}}v^{n+\frac{1}{2}(k)}\right)\right] \tag{4.53}$$

and calculate

$$\|\phi^{n+1(k+1)}-\phi^{n+1(k)}\|_\infty=\epsilon_1. \tag{4.54}$$

(a). Define

$$qq^{n+\frac{1}{2}}:=\left[q^n+\bar{q}_\phi^{n+\frac{1}{2}}\left(\phi^{n+\frac{1}{2}(k+1)}-\phi^n\right)+\bar{q}_e^{n+\frac{1}{2}}\left(e^{n+\frac{1}{2}(k)}-e^n\right)\right]\bar{q}_e^{n+\frac{1}{2}}$$
$$+\gamma_3 e^{n+\frac{1}{2}(k)}; \tag{4.55}$$

(b). substitute $\phi^{n+\frac{1}{2}(k+1)}$, $e^{n+\frac{1}{2}(k)}$ into continuity equation (4.31-4) and equations of the velocity field (4.31-5) and (4.31-6), then use a fast Fourier algorithm coupled with the Neumann boundary condition on $p^{n+\frac{1}{2}}$ to compute $p^{n+\frac{1}{2}}$;

(c). substitute $p^{n+\frac{1}{2}}$ into the equation of the velocity field (4.31-5) and (4.31-6) to solve for $u^{n+\frac{1}{2}(k+1)}$ and $v^{n+\frac{1}{2}(k+1)}$, respectively,

$$
\begin{aligned}
&\left(\frac{2\rho}{\Delta t}-\eta_0\Delta_h\right)u^{n+\frac{1}{2}(k+1)}\\
&=\gamma_1\left[d_xA_x\left(qq^{n+\frac{1}{2}}\left(d_x\phi^{n+\frac{1}{2}(k+1)}\right)^2\right)\right.\\
&\quad\left.+d_yA_y\left(qq^{n+\frac{1}{2}}\left(d_x\phi^{n+\frac{1}{2}(k+1)}\right)\left(a_yD_ya_x\phi^{n+\frac{1}{2}(k+1)}\right)\right)\right]\\
&\quad+\frac{2\rho}{\Delta t}u^n-D_xp^{n+\frac{1}{2}}-\frac{\rho}{2}\left[\left(\bar{u}^{n+\frac{1}{2}}D_x\left(a_xu^{n+\frac{1}{2}(k)}\right)+A_x\left(d_x\left(u^{n+\frac{1}{2}(k)}\bar{u}^{n+\frac{1}{2}}\right)\right)\right.\right.\\
&\quad\left.\left.+a_y\left(A_x\bar{v}^{n+\frac{1}{2}}D_yu^{n+\frac{1}{2}(k)}\right)+d_y\left(A_yu^{n+\frac{1}{2}(k)}A_x\bar{v}^{n+\frac{1}{2}}\right)\right)\right]\\
&\quad+\left(2A_0e^{-2B_0qq^{n+\frac{1}{2}}}-\eta_0\right)\Delta_hu^{n+\frac{1}{2}(k)}+2D_x\left(2A_0e^{-2B_0qq^{n+\frac{1}{2}}}\right)D_x\left(a_xu^{n+\frac{1}{2}(k)}\right)\\
&\quad+A_xD_y\left(2A_0e^{-2B_0qq^{n+\frac{1}{2}}}\right)\left(D_yu^{n+\frac{1}{2}(k)}+A_yd_xv^{n+\frac{1}{2}(k)}\right)+b_1^{n+\frac{1}{2}}
\end{aligned}
\tag{4.56}
$$

and

$$
\begin{aligned}
&\left(\frac{2\rho}{\Delta t}-\eta_0\Delta_h\right)v^{n+\frac{1}{2}(k+1)}\\
&=\gamma_1\left[d_yA_y\left(qq^{n+\frac{1}{2}}\left(d_y\phi^{n+\frac{1}{2}(k+1)}\right)^2\right)\right.\\
&\quad\left.+d_xA_x\left(qq^{n+\frac{1}{2}}\left(d_y\phi^{n+\frac{1}{2}(k+1)}\right)\left(a_xD_ya_y\phi^{n+\frac{1}{2}(k+1)}\right)\right)\right]\\
&\quad+\frac{2\rho}{\Delta t}v^n-D_yp^{n+\frac{1}{2}}-\frac{\rho}{2}\left[\left(\bar{v}^{n+\frac{1}{2}}D_y\left(a_yv^{n+\frac{1}{2}(k)}\right)+A_y\left(d_y\left(v^{n+\frac{1}{2}(k)}\bar{v}^{n+\frac{1}{2}}\right)\right)\right.\right.\\
&\quad\left.\left.+a_y\left(A_x\bar{v}^{n+\frac{1}{2}}D_yu^{n+\frac{1}{2}(k)}\right)+d_y\left(A_yu^{n+\frac{1}{2}(k)}A_x\bar{v}^{n+\frac{1}{2}}\right)\right)\right]\\
&\quad+\left(2A_0e^{-2B_0qq^{n+\frac{1}{2}}}-\eta_0\right)\Delta_hv^{n+\frac{1}{2}(k)}+2D_y\left(2A_0e^{-2B_0qq^{n+\frac{1}{2}}}\right)D_y\left(a_yv^{n+\frac{1}{2}(k)}\right)\\
&\quad+A_yD_x\left(2A_0e^{-2B_0qq^{n+\frac{1}{2}}}\right)\left(D_xv^{n+\frac{1}{2}(k)}+A_xd_yu^{n+\frac{1}{2}(k)}\right)+b_2^{n+\frac{1}{2}},
\end{aligned}
\tag{4.57}
$$

where η_0 is a user-supplied positive constant. Then, we calculate

$$
\left\|u^{n+1^{(k+1)}}-u^{n+1^{(k)}}\right\|_\infty=\epsilon_2,\ \left\|v^{n+1^{(k+1)}}-v^{n+1^{(k)}}\right\|_\infty=\epsilon_3. \tag{4.58}
$$

4. Substitute $\phi^{n+\frac{1}{2}^{(k+1)}}$, $u^{n+\frac{1}{2}^{(k+1)}}$, $v^{n+\frac{1}{2}^{(k+1)}}$ into (4.31-4), then apply a fast Fourier algorithm to compute $e^{n+\frac{1}{2}^{(k+1)}}$,

$$
\begin{aligned}
&\left(\frac{2}{\Delta t}-\theta_0\Delta_h\right)e^{n+\frac{1}{2}(k+1)}\\
&=\frac{2}{\Delta t}e^n-\theta_0\Delta_he^{n+\frac{1}{2}(k)}-\left[d_x\left(A_x\bar{e}^{n+\frac{1}{2}}u^{n+\frac{1}{2}(k+1)}\right)+d_y\left(A_y\bar{e}^{n+\frac{1}{2}}v^{n+\frac{1}{2}(k+1)}\right)\right]\\
&\quad+\gamma_1qq^{n+\frac{1}{2}}\left[d_x\left(A_x\phi^{n+\frac{1}{2}(k+1)}\right)^2d_xu^{n+\frac{1}{2}(k+1)}+d_y\left(A_y\phi^{n+\frac{1}{2}(k+1)}\right)^2d_yv^{n+\frac{1}{2}(k+1)}\right.\\
&\quad\left.+d_x\left(A_x\phi^{n+\frac{1}{2}(k+1)}\right)d_y\left(A_y\phi^{n+\frac{1}{2}(k+1)}\right)\left(a_yD_ya_xu^{n+\frac{1}{2}(k+1)}+a_xD_xa_yv^{n+\frac{1}{2}(k+1)}\right)\right]\\
&\quad+\left(2A_0e^{-2B_0qq^{n+\frac{1}{2}}}\right)\left[\left(d_xu^{n+\frac{1}{2}(k+1)}\right)^2\right.
\end{aligned}
$$

$$+\frac{1}{2}\left(a_x D_x a_y v^{n+\frac{1}{2}(k+1)} + a_y D_y a_x u^{n+\frac{1}{2}(k+1)}\right)^2$$
$$+\left(d_y v^{n+\frac{1}{2}(k+1)}\right)^2\Big] - \Big[d_x\left(A_x\left(\bar{D_e}^{n+\frac{1}{2}}\right)D_x\left(qq^{n+\frac{1}{2}}\right)\right)$$
$$+d_y\left(A_y\left(\bar{D_e}^{n+\frac{1}{2}}\right)D_y\left(qq^{n+\frac{1}{2}}\right)\right)\Big], \tag{4.59}$$

where θ_0 is a sufficiently small positive constant. Then we calculate

$$\left\|e^{n+1^{(k+1)}} - e^{n+1^{(k)}}\right\|_\infty = \epsilon_4. \tag{4.60}$$

5. If

$$max(\epsilon_1, \epsilon_2, \epsilon_3, \epsilon_4) \leq Tol, \tag{4.61}$$

where $Tol = 1 \times 10^{-12}$ is used in our implementation. we set

$$\phi^{n+1} = \phi^{n+1^{(k+1)}}, u^{n+1} = u^{n+1^{(k+1)}}, v^{n+1} = v^{n+1^{(k+1)}}, e^{n+1} = e^{n+1^{(k+1)}}. \tag{4.62}$$

If not, we set $k = k + 1$ and go back to step 2 to repeat the cycle.

Remark 4.1 We apply sine and cosine transforms as fast Fourier algorithms in the implementation to deal with Dirichlet boundary conditions and Neumann boundary conditions, respectively.

4.5 A Decoupled Linear Structure-Preserving Numerical Algorithm Based on the Supplementary Variable Method

Scheme 2 is an algorithm that preserves the volume of each fluid phase, the total energy balance and the entropy-production rate. However, it's weakly nonlinear. To circumvent the issue of nonlinearity, we devise a decoupled, linear, second order, structure-preserving numerical algorithms based on the supplementary variable method. The central idea here is to introduce a supplementary variable to the hydrodynamical phase field model to make the system, consisting of the transport equation of the phase variable, mass, momentum and energy conservation equations, the entropy definition and the entropy-production-rate equation, well-determined. The added degree of freedom in the supplementary variable allows one to enforce the positive entropy production property when the system is discretized. This method extends the idea of a Lagrange multiplier method in the recent paper by Cheng, Liu and Shen [6] for designing unconditionally energy stable schemes for gradient flows. We name the new scheme so derived the supplementary variable scheme (SVM). For simplicity, we only present its semi-discrete version in time here. The spatial discretization using the finite difference method on staggered grid is identical to what we alluded to in Scheme 3 and is omitted.

Scheme 4 **(SVM Scheme)** We use a first order scheme to compute ϕ^1, e^1, q^1. Having obtained ϕ^n, e^n, q^n, we compute $\phi^{n+1}, e^{n+1}, q^{n+1}$ using the following.

$$
\begin{cases}
\rho\delta_t \mathbf{v}^{n+\frac{1}{2}} + \rho\nabla\cdot\left(\bar{\mathbf{v}}^{n+\frac{1}{2}}\mathbf{v}^{n+\frac{1}{2}}\right) = \nabla\cdot\left(2\bar{\eta}^{n+\frac{1}{2}}\mathbf{D}^{n+\frac{1}{2}}\right) - \nabla p^{n+\frac{1}{2}} + \nabla\cdot\sigma_e^{n+\frac{1}{2}} + \mathbf{b}^{n+\frac{1}{2}},\\
\nabla\cdot\mathbf{v}^{n+\frac{1}{2}} = 0,\\
\\
\delta_t\phi^{n+\frac{1}{2}} + \nabla\cdot\left(\overline{\phi}^{n+\frac{1}{2}}\mathbf{v}^{n+\frac{1}{2}}\right) =\\
= -\nabla\cdot\mathbf{M}\nabla\Big(\gamma_1\Delta\phi^{n+\frac{1}{2}} + \big(-2q^{n+\frac{1}{2}}\bar{q}_\phi^{n+\frac{1}{2}} - 2\gamma_2\phi^{n+\frac{1}{2}}\big)\\
\quad +\alpha(t^{n+1/2})\big(-2\overline{q}^{n+\frac{1}{2}}\bar{q}_\phi^{n+\frac{1}{2}} - 2\gamma_2\bar{\phi}^{n+\frac{1}{2}}\big)\Big),\\
\delta_t e^{n+\frac{1}{2}} + \nabla\cdot\left(\bar{e}^{n+\frac{1}{2}}\mathbf{v}^{n+\frac{1}{2}}\right) = \sigma_e^{n+\frac{1}{2}} : \nabla\mathbf{v}^{n+\frac{1}{2}} + 2\bar{\eta}^{n+\frac{1}{2}}\mathbf{D}^{n+\frac{1}{2}} : \nabla\mathbf{v}^{n+\frac{1}{2}}\\
+2\nabla\cdot\left[\bar{D}_e^{n+\frac{1}{2}}\nabla\big(q^{n+\frac{1}{2}}\bar{q}_e^{n+\frac{1}{2}} + \gamma_3 e^{n+\frac{1}{2}}\big)\right] + 2\alpha(t^{n+1/2})\nabla\cdot\left[\bar{D}_e^{n+\frac{1}{2}}\nabla\big(\bar{q}^{n+\frac{1}{2}}\bar{q}_e^{n+\frac{1}{2}} + \gamma_3\bar{e}^{n+\frac{1}{2}}\big)\right],\\
\delta_t q^{n+\frac{1}{2}} = \bar{q}_\phi^{n+\frac{1}{2}}\delta_t\phi^{n+\frac{1}{2}} + \bar{q}_e^{n+\frac{1}{2}}\delta_t e^{n+\frac{1}{2}},\\
\\
\frac{S(\phi^{n+1},e^{n+1},q^{n+1}) - S\left(\phi^n,e^n,q^n\right)}{\Delta t}\\
= \int_\Omega\left[M\left(\nabla\frac{\delta S^{n+\frac{1}{2}}}{\delta\phi}\right)^2 + 2\bar{\eta}^{n+\frac{1}{2}}\left(\frac{1}{T}\right)^{n+\frac{1}{2}}\mathbf{D}^{n+\frac{1}{2}} : \mathbf{D}^{n+\frac{1}{2}} + \bar{D}_e^{n+\frac{1}{2}}|\nabla\frac{\delta S^{n+\frac{1}{2}}}{\delta e}|^2\right]d\mathbf{x}.
\end{cases}
\tag{4.63}
$$

where

$$
\begin{cases}
\sigma_e^{n+\frac{1}{2}} = \frac{\gamma_1\nabla\overline{\phi}^{n+\frac{1}{2}}\nabla\overline{\phi}^{n+\frac{1}{2}}}{2\left(\bar{q}^{n+\frac{1}{2}}\bar{q}_e^{n+\frac{1}{2}} + \gamma_3\bar{e}^{n+\frac{1}{2}}\right)}, \quad \bar{\eta}^{n+\frac{1}{2}} = A_0 e^{\left(\frac{B_0}{T}\right)^{n+\frac{1}{2}}} = A_0 e^{-2B_0\left(\bar{q}^{n+\frac{1}{2}}\bar{q}_e^{n+\frac{1}{2}} + \gamma_3\bar{e}^{n+\frac{1}{2}}\right)},\\
\bar{D}_e^{n+\frac{1}{2}} = D_0\left(\frac{1}{C_A}\left[\bar{e}^{n+\frac{1}{2}} - e_A(T_M) - \big(p\big(\bar{\phi}^{n+\frac{1}{2}}\big) - 1\big)L_0\right] + T_M\right)^2,\\
S\left(\phi^n, e^n, q^n\right) = \int_\Omega\left[-|q^n|^2 - \gamma_2|\phi^n|^2 - \gamma_3|e^n|^2 - \frac{\gamma_1}{2}|\nabla\phi^n|^2 + C_0\right]d\mathbf{x}.
\end{cases}
\tag{4.64}
$$

Remark 4.2 Supplementary variable $\alpha(t^{n+1/2})$ can also be viewed as a perturbation variable since when $\alpha(t) = 0$, the modifed/perturbed PDE system reduces to the original one. In the implementation, the governing equation for $\alpha(t^{n+1/2})$ is quadratic since $S(\phi, e, q)$ is quadratic. So, $\alpha(t^{n+1/2})$ is solved analytically. The numerical cost for this step is negligible. Eq.(4.63-6) indicates that the scheme automatically preserves the positive entropy production rate.

Theorem 4.3 *1. Under boundary conditions (4.15), Scheme 4 preserves the total energy balance:*

$$E^{n+1} - E^n = \int_\Omega \mathbf{b}^{n+\frac{1}{2}}\cdot\mathbf{v}^{n+\frac{1}{2}}d\mathbf{x}, \tag{4.65}$$

where

$$E^n = \int_\Omega\left[e^n + \frac{\rho}{2}|\mathbf{v}^n|^2\right]d\mathbf{x}. \tag{4.66}$$

If $\mathbf{b}^{n+\frac{1}{2}}$*=0,* $E^{n+1} = E^n$*, i.e., Scheme 4 conserves the total energy.*

2. Scheme 4 preserves the volume of fluid A:

$$V^{n+1} = V^n, \tag{4.67}$$

where

$$V^n = \int_\Omega \phi^n d\mathbf{x}. \tag{4.68}$$

Since the proof of this Theorem is similar to that in Theorem 4.1, we omit the details.

Although this scheme seems to be nonlinear, it in fact decouples the energy balance equation from the rest of the equations in the system. It is therefore a linear scheme. We detail its implementation as follows.

Scheme 5 **(Implementation of the SVM scheme)** Having obtained ϕ^n, e^n, q^n, we compute ϕ^{n+1}, e^{n+1}, q^{n+1} as follows.

- Firstly, we solve $\mathbf{v}^{n+1}$ from (4.63-1);
- Secondly, from the equation for q^{n+1}, we obtain

$$q^{n+\frac{1}{2}} = q^n + \frac{1}{2}\bar{q}_\phi^{n+\frac{1}{2}}\left(\phi^{n+1} - \phi^n\right) + \frac{1}{2}\bar{q}_e^{n+\frac{1}{2}}\left(e^{n+1} - e^n\right). \tag{4.69}$$

Substituting Eq. (4.69) into (4.63), we arrive at a linear system for (ϕ^{n+1}, e^{n+1}). We decompose (ϕ^{n+1}, e^{n+1}) into

$$\phi^{n+1} = \phi_1^{n+1} + \alpha\phi_2^{n+1}, \quad e^{n+1} = e_1^{n+1} + \alpha e_2^{n+1}, \tag{4.70}$$

where $(\phi_1^{n+1}, e_1^{n+1})$ is the solution of

$$\begin{cases} \frac{1}{\Delta t}(\phi_1^{n+1} - \phi^n) + \nabla\cdot\left(\overline{\phi}^{n+\frac{1}{2}}\mathbf{v}^{n+\frac{1}{2}}\right) \\ = -\nabla\cdot\mathbf{M}\nabla\left(\gamma_1\Delta\frac{\phi_1^{n+1}+\phi^n}{2} + \left(-2q_1^{n+\frac{1}{2}}\bar{q}_\phi^{n+\frac{1}{2}} - 2\gamma_2\frac{\phi_1^{n+1}+\phi^n}{2}\right)\right), \\ \frac{1}{\Delta t}\left(e_1^{n+1} - e^n\right) + \nabla\cdot\left(\overline{e}^{n+\frac{1}{2}}\mathbf{v}^{n+\frac{1}{2}}\right) \\ = \sigma_e^{n+\frac{1}{2}} : \nabla\mathbf{v}^{n+\frac{1}{2}} + 2\bar{\eta}^{n+\frac{1}{2}}\mathbf{D}^{n+\frac{1}{2}} : \nabla\mathbf{v}^{n+\frac{1}{2}} \\ \quad +2\nabla\cdot\left[\bar{D}_e^{n+\frac{1}{2}}\nabla\left(q_1^{n+\frac{1}{2}}\bar{q}_e^{n+\frac{1}{2}} + \gamma_3\frac{e_1^{n+1}+e^n}{2}\right)\right], \end{cases} \tag{4.71}$$

with $q_1^{n+\frac{1}{2}} = q^n + \frac{1}{2}\bar{q}_\phi^{n+\frac{1}{2}}(\phi_1^{n+1} - \phi^n) + \frac{1}{2}\bar{q}_e^{n+\frac{1}{2}}(e_1^{n+1} - e^n)$, and $(\phi_2^{n+1}, e_2^{n+1}, q_2^{n+1})$ is the solution of

$$\begin{cases} \frac{1}{\Delta t}\phi_2^{n+1} = -\nabla\cdot\mathbf{M}\nabla\left(\gamma_1\Delta\frac{\phi_2^{n+1}}{2} + \left(-2q_2^{n+\frac{1}{2}}\bar{q}_\phi^{n+\frac{1}{2}} - 2\gamma_2\frac{\phi_2^{n+1}}{2}\right)\right. \\ \quad \left. + \left(-2\overline{q}^{n+\frac{1}{2}}\bar{q}_\phi^{n+\frac{1}{2}} - 2\gamma_2\bar{\phi}^{n+\frac{1}{2}}\right)\right), \\ \frac{1}{\Delta t}e_2^{n+1} = 2\nabla\cdot\left[\bar{D}_e^{n+\frac{1}{2}}\nabla\left(q_2^{n+\frac{1}{2}}\bar{q}_e^{n+\frac{1}{2}} + \gamma_3\frac{e_2^{n+1}}{2}\right)\right] \\ \quad +2\nabla\cdot\left[\bar{D}_e^{n+\frac{1}{2}}\nabla\left(\bar{q}^{n+\frac{1}{2}}\bar{q}_e^{n+\frac{1}{2}} + \gamma_3\bar{e}^{n+\frac{1}{2}}\right)\right], \end{cases} \tag{4.72}$$

with $q_2^{n+\frac{1}{2}} = \frac{1}{2}\bar{q}_\phi^{n+\frac{1}{2}}\phi_2^{n+1} + \frac{1}{2}\bar{q}_e^{n+\frac{1}{2}}e_2^{n+1}$.

- Thirdly, we solve for $\alpha(t^{n+1/2})$ from its governing equation. We define

$$\begin{aligned} EPR\left(\phi^{n+1}, e^{n+1}, q^{n+1}\right) &= \frac{S\left(\phi^{n+1}, e^{n+1}, q^{n+1}\right) - S\left(\phi^n, e^n, q^n\right)}{\Delta t} \\ &= \int_\Omega \left[M\left(\nabla\frac{\delta S^{n+\frac{1}{2}}}{\delta\phi}\right)^2 | + 2\bar{\eta}^{n+\frac{1}{2}}\left(\frac{1}{T}\right)^{n+\frac{1}{2}}\mathbf{D}^{n+\frac{1}{2}} : \mathbf{D}^{n+\frac{1}{2}} + \bar{D}_e^{n+\frac{1}{2}}|\nabla\frac{\delta S^{n+\frac{1}{2}}}{\delta e}|^2| \right] dx \end{aligned} \tag{4.73}$$

and

$$\int_\Omega \left(\frac{\delta S}{\delta e}, \frac{\delta S}{\delta q}, \phi, \nabla\phi\right)|_{(\bullet)_1} \cdot \left(\frac{\delta S}{\delta e}, \frac{\delta S}{\delta q}, \phi, \nabla\phi\right)|_{(\bullet)_2} d\mathbf{x}$$
$$= \int_\Omega \left(\frac{\delta S}{\delta e}, \frac{\delta S}{\delta q}, \phi, \nabla\phi\right)|_{\left(\phi_1^{n+1}, e_1^{n+1}, q_1^{n+1}\right)} \cdot \left(\frac{\delta S}{\delta e}, \frac{\delta S}{\delta q}, \phi, \nabla\phi\right)|_{\left(\phi_2^{n+1}, e_2^{n+1}, q_2^{n+1}\right)} d\mathbf{x}$$
$$= \int_\Omega \left(q_1^{n+1} q_2^{n+1} + \gamma_2 \phi_1^{n+1}\phi_2^{n+1} + \gamma_3 e_1^{n+1} e_2^{n+1} + \frac{\gamma_1}{2}\nabla\phi_1^{n+1}\nabla\phi_2^{n+1}\right) dx. \quad (4.74)$$

where EPR stands for entropy-production-rate and $(\bullet) = (\phi^{n+1}, e^{n+1}, q^{n+1})$. $\alpha(t^{n+1/2})$ is governed by the following quadratic equation

$$\alpha^2 \left[\left(S\left(\phi_2^{n+1}, e_2^{n+1}, q_2^{n+1}\right) - \int_\Omega C_0 d\mathbf{x}\right) - \frac{\Delta t}{4}\int_\Omega \left[M \|\nabla \frac{\delta S}{\delta \phi}|_{\left(\phi_2^{n+1}, q_2^{n+1}\right)}\|^2 \right.\right.$$
$$\left.\left. \bar{D_e}^{n+1/2} \|\nabla \frac{\delta S}{\delta e}|_{\left(e_2^{n+1}, q_2^{n+1}\right)}\|^2 \right] d\mathbf{x} \right]$$
$$-2\alpha \left[\int_\Omega \left(\frac{\delta S}{\delta e}, \frac{\delta S}{\delta q}, \phi, \nabla\phi\right)|_{(\bullet)_1} \cdot \left(\frac{\delta S}{\delta e}, \frac{\delta S}{\delta q}, \phi, \nabla\phi\right)|_{(\bullet)_2} d\mathbf{x} \right.$$
$$- \frac{\Delta t}{2}\int_\Omega M \nabla\left(\frac{\delta S}{\delta \phi}|_{\phi_1^{n+1}, q_1^{n+1}}\right) \cdot \nabla\left(\frac{\delta S}{\delta \phi}|_{\phi_2^{n+1}, q_2^{n+1}}\right) + \bar{D_e}^{n+1/2} \nabla\left(\frac{\delta S}{\delta e}|_{e_1^{n+1}, q_1^{n+1}}\right)$$
$$\left. \cdot \nabla\left(\frac{\delta S}{\delta e}|_{e_2^{n+1}, q_2^{n+1}}\right) d\mathbf{x} \right] + S\left(\phi_1^{n+1}, e_1^{n+1}, q_1^{n+1}\right) - S\left(\phi^n, e^n, q^n\right)$$
$$-\Delta t\, EPR\left(\phi_1^{n+1}, e_1^{n+1}, q_1^{n+1}\right) = 0. \quad (4.75)$$

We choose the root closer to zero as the solution of the quadratic equation.
An alternative is to define the discrete entropy production rate by

$$\frac{S\left(\phi^{n+1}, e^{n+1}, q^{n+1}\right) - S\left(\phi^n, e^n, q^n\right)}{\Delta t} = EPR\left(\phi_1^{n+1}, e_1^{n+1}, q_1^{n+1}\right). \quad (4.76)$$

Then the equation for $\alpha(t^{n+1/2})$ is given by

$$\alpha^2 \left(S\left(\phi_2^{n+1}, e_2^{n+1}, q_2^{n+1}\right) - \int_\Omega C_0 d\mathbf{x}\right) - 2\alpha \int_\Omega \left(\frac{\delta S}{\delta e}, \frac{\delta S}{\delta q}, \phi, \nabla\phi\right)|_{(\bullet)_1}$$
$$\cdot \left(\frac{\delta S}{\delta e}, \frac{\delta S}{\delta q}, \phi, \nabla\phi\right)|_{(\bullet)_2} d\mathbf{x} + S\left(\phi_1^{n+1}, e_1^{n+1}, q_1^{n+1}\right)$$
$$-S\left(\phi^n, e^n, q^n\right) - \Delta t\, EPR\left(\phi_1^{n+1}, e_1^{n+1}, q_1^{n+1}\right) = 0. \quad (4.77)$$

- Finally, we update $\phi^{n+1}, e^{n+1}, q^{n+1}$ via

$$\phi^{n+1} = \phi_1^{n+1} + \alpha\phi_2^{n+1}, e^{n+1} = e_1^{n+1}$$
$$+ \alpha e_2^{n+1}, q^{n+1} = q^n + \bar{q}_\phi^{n+\frac{1}{2}}\left(\phi^{n+1} - \phi^n\right) + \bar{q}_e^{n+\frac{1}{2}}\left(e^{n+1} - e^n\right). \quad (4.78)$$

Theorem 4.4 *If*

$$\int_\Omega \left(\frac{\delta S}{\delta e}, \frac{\delta S}{\delta q}, \phi, \nabla\phi\right)|_{(\bullet)_1} \cdot \left(\frac{\delta S}{\delta e}, \frac{\delta S}{\delta q}, \phi, \nabla\phi\right)|_{(\bullet)_2} d\mathbf{x} \neq 0, \quad (4.79)$$

there exists a $\tau > 0$ such that (4.77) admits a solution close to zero when $0 < \Delta t < \tau$. The SVM scheme is second order in both space and time and $\alpha(t^{n+1/2}) \sim O(\Delta t^2)$.

Proof The existence follows from the expression of the linear term in (4.77). It follows from the second order approximation of the scheme to the PDE system at $\alpha = 0$ that

$$S\left(\phi_1^{n+1}, e_1^{n+1}, q_1^{n+1}\right) - S\left(\phi^n, e^n, q^n\right) - \Delta t EPR\left(\phi_1^{n+1}, e_1^{n+1}, q_1^{n+1}\right) = O(\Delta t^3). \quad (4.80)$$

A simple analysis of the quadratic equation (4.77) yields

$$\alpha\left(t^{n+1/2}\right)\|(\bullet)_2\| \sim O(\Delta t^3), \quad (4.81)$$

where $(\bullet)_2 = \left(\phi_2^{n+1}, e_2^{n+1}, q_2^{n+1}\right)$. It follows from $\|(\bullet)_2\| \sim O(\Delta t)$ that

$$\alpha(t^{n+1/2}) \sim O(\Delta t^2). \quad (4.82)$$

□

5 Numerical Results and Discussions

In this section, we conduct several numerical experiments to confirm the accuracy of the schemes firstly and then show usefulness of the numerical schemes and their entropy-production-rate preserving properties in simulating the thermal induced hydrodynamics in a two immiscible viscous fluid system. We adopt the following adiabatic boundary conditions:

$$\mathbf{n} \cdot \nabla\phi \mid_{\partial\Omega} = 0, \mathbf{n} \cdot \mathbf{q} = 0, \mathbf{n} \cdot \nabla e \mid_{\partial\Omega} = 0, u|_{\partial\Omega} = 0, v|_{\partial\Omega} = 0. \quad (5.1)$$

5.1 Accuracy Test

In order to test the temporal convergence rate, we set the model parameter values as follows

$$M = 10^{-3}, \gamma_1 = 10^{-3}, \gamma_2 = 10^2, C_0 = 10^3, \rho = 1, \gamma_3 = 10^{-2}, L_x = L_y = 1,$$
$$C_A = 0.6, T_M = 1, e_A(T_M) = 0, L_0 = 0.5, D_0 = 6 \times 10^{-3}, A_0 = 1, B_0 = 1, \quad (5.2)$$

with initial conditions

$$T(x, y, 0) = 3T_M + T_M \tanh\left(\frac{1-y}{0.01}\right) + T_M \cos(2\pi x),$$
$$\phi(x, y, 0) = \frac{1}{2}\left[1 + \tanh\left(\frac{y-0.5}{0.02}\right)\right], \quad u(x, y, 0) = 0, \quad v(x, y, 0) = 0. \quad (5.3)$$

We use the difference between results on successive coarse and finer grids to evaluate the numerical error. The computation is carried out in rectangular domain $\Omega = [0, L_x] \times [0, L_y]$ with mesh size $N_x = N_y = 128$ and time step $\Delta t = 10^{-4} \times \frac{1}{2^{k-1}}, k = 1, 2, 3, \ldots$, respectively. The error shown is the L^2 norm of the difference of quantity $\sqrt{\phi^2 + e^2}$, $\sqrt{u^2 + v^2}$ and p between consecutive grid sizes. The mesh refinement test results are summarized in Fig. 1a–c for temporal mesh refinement. The results clearly demonstrate the second-order convergence rate in time for the EQ Scheme and the SVM Scheme.

In order to test the spatial convergence rate, we set the model parameter values as

$$M = 10^{-5}, \gamma_1 = 10^{-2}, \gamma_2 = 10^2, C_0 = 10^3, \rho = 1, \gamma_3 = 10^2, L_x = L_y = 1,$$
$$C_A = 0.6, T_M = 1, e_A(T_M) = 0, L_0 = 0.5, D_0 = 6 \times 10^{-5}, A_0 = 1, B_0 = 1, \quad (5.4)$$

and initial conditions

$$T(x, y, 0) = 0.5T_M, \quad u(x, y, 0) = 0,$$

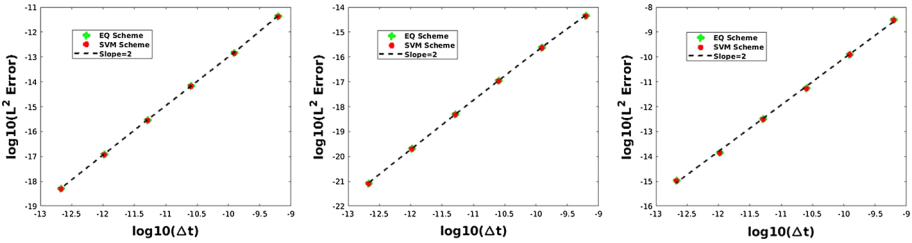

(a) $\sqrt{\phi^2 + e^2}$ **(b)** $\|\mathbf{v}\|_2 = \sqrt{u^2 + v^2}$ **(c)** p

Fig. 1 Mesh refinement in time for the two schemes. **a** The L_2 error of $\sqrt{\phi^2 + e^2}$. **b** The L_2 error of $\|\mathbf{v}\|_2 = \sqrt{u^2 + v^2}$. **c** The L_2 error of pressure p. Here, we fix the number of spatial meshes at $N_x = N_y = 128$. Second order convergence rates in time are confirmed

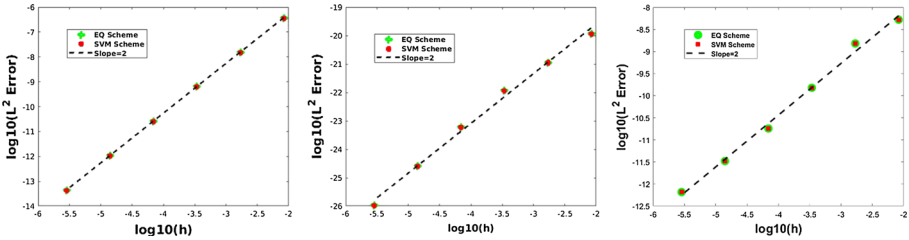

(a) $\sqrt{\phi^2 + e^2}$ **(b)** $\|\mathbf{v}\|_2 = \sqrt{u^2 + v^2}$ **(c)** p

Fig. 2 Mesh refinement in space for the two schemes. **a** The L_2 error of $\sqrt{\phi^2 + e^2}$. **b** The L_2 error of $\|\mathbf{v}\|_2 = \sqrt{u^2 + v^2}$. **c** The L_2 error of pressure p. Here, we fix the time step at $\Delta t = 1.0 \times 10^{-5}$. Second order convergence rates in space are confirmed

$$\phi(x, y, 0) = \frac{1}{2} + \frac{1}{2}\cos(\pi x)\cos(\pi y), \quad v(x, y, 0) = 0. \tag{5.5}$$

The computation domain is $\Omega = [0, L_x] \times [0, L_y]$, time step $\Delta t = 1.0 \times 10^{-5}$ and mesh size $N_x = N_y = 8 \times 2^k$, $k = 0, 1, 2, 3, \ldots$, respectively. We calculate the L^2 norm of the difference of $\sqrt{\phi^2 + e^2}$, $\sqrt{u^2 + v^2}$ and p between consecutive grid sizes as errors. The mesh refinement test results are summarized in Fig. 2a–c for spatial mesh refinement. The second-order convergence rate is clearly established for the EQ Scheme and the SVM Scheme in space. From Figs. 1 and 2, we conclude that the proposed schemes indeed possesses a second order convergence rate in both time and space.

We next use the code based on the EQ scheme to study thermocapillary convection in a binary immiscible viscous fluid in an adiabatic container.

5.2 Thermocapillary Convection in an Immiscible Binary Viscus Fluid System

We consider thermocapillary convection of two-layer, superimposed viscous fluids subject to a temperature gradient at their interface without the gravity effect ($\mathbf{b} = 0$). The flow geometry is shown in Fig. 3, where immiscible fluids A and B are placed one on top of the other with a flat interface initially. We note that the system we consider here has no heat exchange with the outside, the adiabatic boundary conditions for the temperature (or the internal energy) and

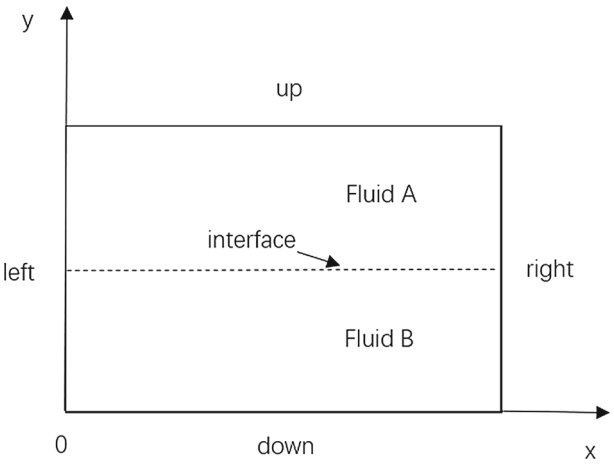

Fig. 3 Sketch of the physical domain for the two-layer fluid system

phase variables are Neumann and those for the velocity are Dirichlet. The physical properties of the fluids are described by their densities, temperature and viscosities, respectively. We assume that only the fluid viscosities and the surface tension are affected by the temperature variation in the range of temperature we consider in this study.

We identify fluid A as Acetonitrile and fluid B as n-Hexane in this study and consider the computational domain in a rectangle $\Omega = [0, L_x] \times [0, L_y]$ with $L_x = L_y = 20$ mm. In Table 5.9, we list the values of the physical parameters of the two fluid components [16], where $\nu = \frac{\eta}{\rho}$ is the kinematic viscosity, C is the specific heat, σ is the surface tension parameter. Note that the melting and boiling points of Acetonitrile are 225 K and 354.4 K, and those of n-Hexane are 179 K and 346 K, respectively. So both are in liquid phase between 225 and 346 K. In the following, we use characteristic length scale $l_0 = 2 \times 10^{-2}$ m, time scale $t_0 = 2 \times 10^{-4}$ s, density scale $\rho_0 = 0.776 \times 10^3\,\mathrm{kg \cdot m^{-3}}$ and temperature scale $T_0 = 230$ K to nondimensionalize the equation system and then perform numerical simulations using the dimensionless equations. We impose the initial temperature field, the velocity field and pressure field as follows

$$\begin{aligned} &T(x, y, 0) = T_a + T_b[1 + \cos(\omega x)], \\ &p(x, y, 0) = 0; u(x, y, 0) = 0; v(x, y, 0) = 0, 0 \le x \le L_x, 0 \le y \le L_y, \end{aligned} \tag{5.6}$$

where $\omega = \frac{2\pi}{l}(0 \le l \le L_x)$ is a wave number parameter. By adjusting the parameter, we can vary temperature in the horizontal direction to impose spatial gradients initially.

Since the problem setting is in an adiabatic container, the thermocapillary effect is going to be induced by the initial temperature gradient. First of all, we consider an initial temperature gradient parallel to the fluid interface and the initial condition of phase variable is given by

$$\phi(x, y, 0) = \frac{1}{2} + \frac{1}{2} \tanh\left(\frac{y - 0.5}{\epsilon}\right), 0 \le y \le 1, \tag{5.7}$$

where ϵ is the thickness of the diffuse interface. In addition, we set dimensional $T_a = 230K$ and $T_b = 23K$ in (5.6). Then, the dimensionless temperature $T_a = 1$ and $T_b = 0.1$. In addition, we use $\omega = 2\pi, 4\pi$ to impose the temperature gradient in the domain, respectively.

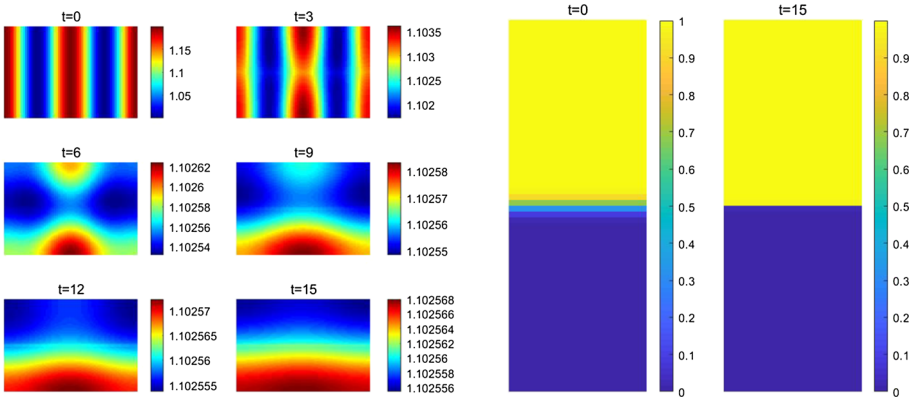

(a) Temperature field T. **(b)** Phase field ϕ.

Fig. 4 Snapshots of the temperature and phase field at selected times in thermocapillary convection with an initial temperature gradient parallel to the interface ($\omega = 4\pi$). **a** The temperature field at $t = 0, 3, 6, 9, 12, 15$, respectively. **b** The phase field at $t = 0$ and $t = 15$, respectively. The interface becomes sharper as the temperature gradient reduces while remaining flat during the process

Other model parameter values are chosen as follows

$$M = 10^{-3}, L_x = L_y = 1, C_0 = 10^3, \rho = 1, C_A = 0.066, T_M = 1, e_A(T_M) = 0, \epsilon = 0.02$$
$$A_0 = 5 \times 10^{-3}, B_0 = 1, D_0 = 1.78 \times 10^{-2}, \gamma_1 = 10^{-3}, \gamma_2 = 10^2, \gamma_3 = 10^{-2}, L_0 = 0.5. \tag{5.8}$$

In the simulations, we use $N_x = N_y = 128$ meshes in space, time step $\Delta t = 1.0 \times 10^{-4}$ and solve the problem until $t = 40$ for $\omega = 2\pi$ and $t = 15$ for $\omega = 4\pi$, respectively.

Observed from the temperature distribution at different moment in Figs. 4a and 7a for different wave numbers, we notice that there are different patterns of temperature gradients along the interface corresponding to different initial temperature profiles. Owing to both convection and dissipation, the temperature gradient gradually reaches zero in the system. Initially, each temperature fluctuation creates a circular fluid flow pattern, known as a roll cell. For instance, at $\omega = 4$, there are four roll cells initially, in which velocity fields in each pair rotate in opposite directions. The roll cells merge into larger roll cells as the temperature gradient dissipates. These phenomena are shown in Figs. 5a and 6a. Figure 4a shows snapshots of numerical simulations of the temperature field at $t = 0, 3, 6, 9, 12, 15$, respectively, with wave number $\omega = 4\pi$, and Fig. 5 presents the snapshots of the velocity field at $t = 0.001, 3, 6, 12$, respectively, with wave number $\omega = 4\pi$. Analogously, Fig. 7a depicts snapshots of numerical simulations of the temperature field at $t = 0, 8, 16, 24, 32, 40$, with wave number $\omega = 2\pi$ while Fig. 6 presents snapshots of flow field at $t = 1, 16, 24, 40$, with wave number $\omega = 2\pi$. Figure 4b shows the phase field at the initial time $t = 0$ and $t = 15$ with $\omega = 4\pi$, respectively. Figure 7b presents the phase field at the initial time $t = 0$ and $t = 40$ with $\omega = 2\pi$, respectively.

During the simulation, we notice that the interface between the two fluids remains flat, which is also verified by the distribution of the velocity field in Figs. 5 and 6. Finally, Figs. 8 and 9 confirm that the system preserves both the total energy, volume and the positive entropy production rate. These numerical results demonstrate that the initial temperature gradient in the horizontal direction induces a shear force along the interface, which leads to

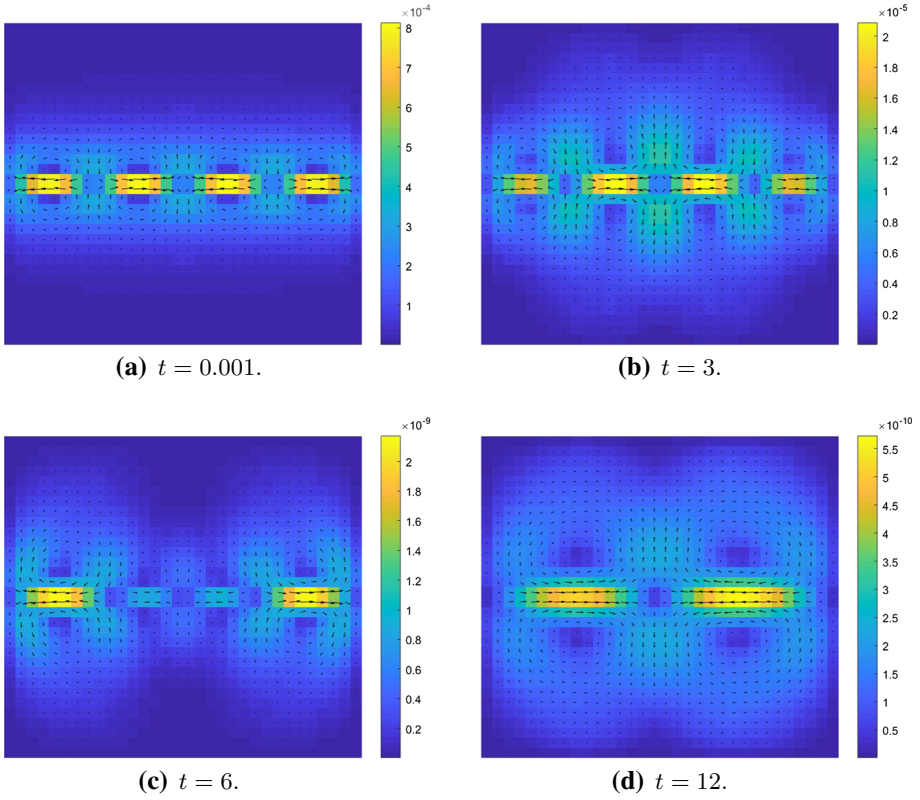

(a) $t = 0.001$. **(b)** $t = 3$.

(c) $t = 6$. **(d)** $t = 12$.

Fig. 5 Snapshots of the velocity field at selected times in thermocapillary convection with an initial temperature gradient parallel to the interface ($\omega = 4\pi$). **a** **v** at t $= 0.001$. **b** **v** at t $= 3$. **c** **v** at t $= 6$. **d** **v** at t $= 12$. Initially, there are four roll cells in the neighborhood of the interface shown in (**a**). As the temperature gradient reduces, the number of roll cells reduces as well (see **c**, **d**). It demonstrates that the thermocapillary convection drives the roll cell reduction. As the temperature reaches an average temperature after a long time, the roll cell reduction phenomena ceases as well

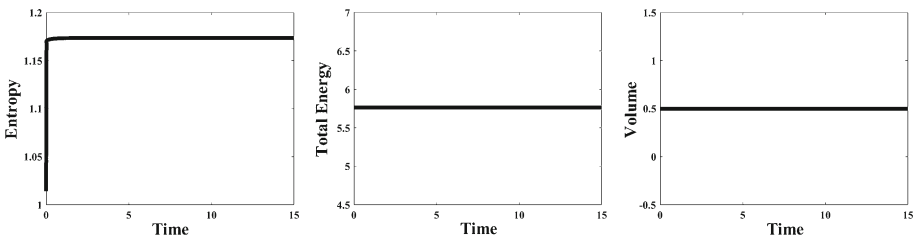

(a) Entropy S. **(b)** Total energy E. **(c)** The volume V.

Fig. 6 Evolution of the entropy, total energy and volume of the system over time ($\omega = 4\pi$). **a** The entropy S. **b** The total energy E. **c** The volume V. It demonstrates that the scheme preserves the thermodynamic consistency and the volume

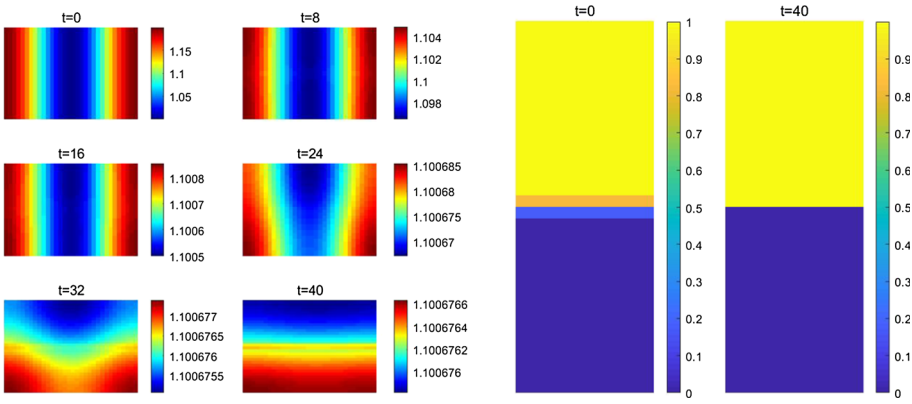

(a) Temperature field T. **(b)** Phase field ϕ.

Fig. 7 Snapshots of the temperature and phase field at selected times in thermocapillary convection with an initial temperature gradient parallel to the interface ($\omega = 2\pi$). **a** The temperature field at $t = 0, 8, 16, 24, 32, 40$, respectively. **b** The phase field at $t = 0$ and $t = 40$, respectively. The interface becomes sharper as the temperature gradient reduces while remaining flat during the process

the formation of circulating roll cells. However, the shear force is so weak and parallel to the flat fluid interface that it does not disrupt the fluid interface in this case.

Next, we simulate the binary fluid system with the fluid interface perpendicular to the initial temperature gradient. In order to maximize the temperature effect to the system, we set $T_a = 1$ and $T_b = 0.25$. So, in this case, the temperature gradient is the largest at $x = \frac{3}{8}$ and the dimensionless initial condition of the phase variable is given by

$$\phi(x, y, 0) = \frac{1}{2} + \frac{1}{2}\tanh\left(\frac{x - 0.375}{\epsilon}\right), 0 \le x \le 1, \tag{5.9}$$

where ϵ is the thickness of the diffuse interface. All the other initial values and parameters are the same as in the previous case. Here, we choose $N_x = N_y = 128$ meshes in space, time step $\Delta t = 1.0 \times 10^{-4}$ and solve the problem until time $t = 10$. Figure 10a shows the snapshots of numerical simulations of temperature field at $t = 0, 2, 4, 6, 8, 10$ and Fig. 11 presents the snapshots of flow field at $t = 0.01, 2, 6, 8$. Figure 10b presents the phase field at time $t = 0$ and $t = 10$, respectively.

The interfacial tension is estimated using Antonow's rule [1], which states that the interfacial tension between two liquids is equal to the difference between their surface tensions in air. Thus, from Table 1, we include the interfacial tension at the interface between Acetonitrile and n-Hexane at 1.077×10^{-2} N/m. Due to different temperatures on each side of the interface, forces are generated in the direction perpendicular to the interface, resulting in deformation of the interface. However, under the weak temperature difference in this particular case, the maximum viscous force numerically obtained is $O(10^{-5})$ (N/m), this value is too small to overcome the surface tension. So, the temperature gradient induced viscous force is not sufficient to cause any changes in the interface during the simulation. Since the system is dissipative, the gradient dissipates over time so that interface remains flat all the time in the simulation. From Fig. 11, we observe that the velocity direction in the roll cells at the interface is parallel to the interface, verified by the distribution of the phase field in Fig. 10b.

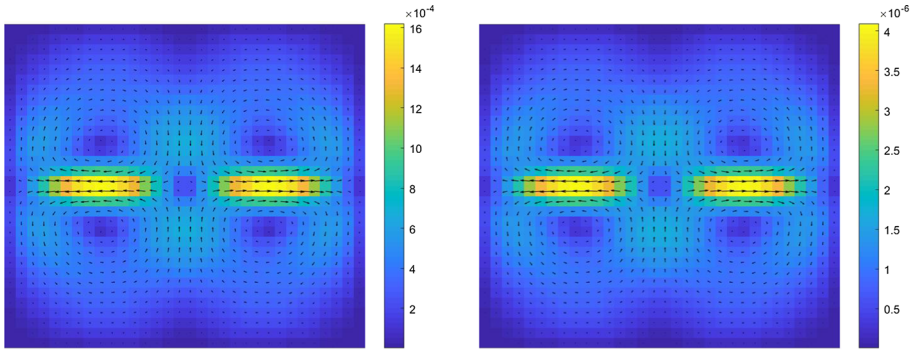

(a) $t = 1$. **(b)** $t = 16$.

(c) $t = 24$. **(d)** $t = 40$.

Fig. 8 Snapshots of the velocity field at selected times in thermocapillary convection with an initial temperature gradient parallel to the interface ($\omega = 2\pi$). **a** **v** at t $= 1$. **b** **v** at t $= 16$. **c** **v** at t $= 24$. **d** **v** at t $= 40$. Initially, there are two roll cells in the neighborhood of the interface shown in (**a**). As the temperature gradient reduces, the number of roll cells reduces (see **c, d**). It demonstrates that the thermocapillary effect drives the roll cell reduction. As the temperature reaches an average temperature after a long time, the roll cell reduction phenomena ceases as well

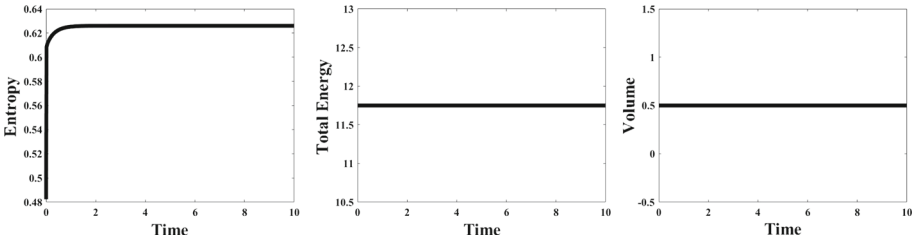

(a) Entropy S. **(b)** Total energy E. **(c)** Volume V.

Fig. 9 Evolution of the entropy, total energy and volume of the system over time ($\omega = 2\pi$). **a** The entropy S. **b** The total energy E. **c** The volume V. It demonstrates that the scheme preserves the thermodynamic consistency and the volume

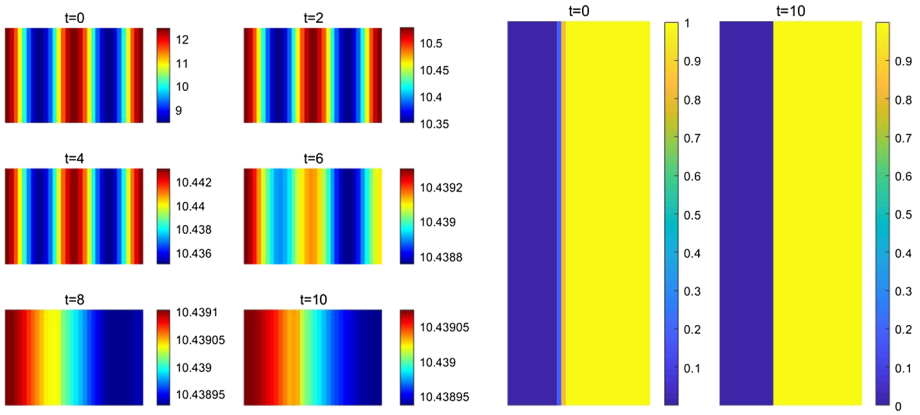

(a) Temperature field T. **(b)** Phase field ϕ.

Fig. 10 Snapshots of the temperature field and phase field at selected times with an initial temperature gradient perpendicular to the interface, where the interface is at $x = \frac{3}{8}$. **a** The temperature field at $t = 0, 2, 4, 6, 8, 10$, respectively. **b** The phase field at $t = 0$ and $t = 10$, respectively. Due to the relatively small temperature difference across the interface, surface tension still dominates the temperature-induced viscous shear stress so that the interface is intact in the simulation despite the existence of weak flows leading to roll cells in the neighborhood of the interface

Finally, we consider a suspending circular drop of fluid B with radius 1/4 immersed in fluid A to demonstrate the thermal effect on hydrodynamics of the binary fluid system and in particular to the fluid interface. The initial condition of the phase variable is given by

$$\phi(x, y, 0) = \begin{cases} 1, & r \le 0.25 - \delta, \\ \tanh\left(\frac{0.25-r}{\delta}\right), & 0.25 - \delta < r \le 0.25 + \delta, \\ 0, & \text{other}, \end{cases} \tag{5.10}$$

where $r = \sqrt{(x-0.5)^2 + (y-0.5)^2}$ and $\delta = 0.01$.

We take the dimensionless initial temperature field under the maximum temperature difference as $T_a = 1$ and $T_b = 0.25$ in (5.6). All the other initial values and parameters are chosen the same as before. From Fig. 12a, we observe the temperature gradient at moment $t = 0$ and $t = 2$. The corresponding velocity field are shown in Fig. 13a and b, respectively. Owing to energy dissipation, the temperature gradient decays rapidly, during which flow cells form at the interface instead of in the bulk. This phenomenon is also shown in Fig. 13c, d. Figure 12a shows the snapshot of numerical simulations of the temperature field at $t = 0, 2, 4, 6, 8, 10$, respectively; (b) shows the snapshot of numerical simulations of phase field at $t = 0, 2, 4, 6, 8, 10$, respectively. Figure 13 presents the snapshot of flow field at $t = 1, 2, 8, 10$, respectively.

The simulation documents the temperature field changes with time from Fig. 12a, b, which are also verified by the distribution of the velocity field in Fig. 13. Figure 14 confirms that the system preserves the total energy, volume and the positive entropy production rate. The heat induced capillary flow is along the interface so that the interface becomes fuzzy during some moment in the simulation and recovers after the temperature gradient reduces.

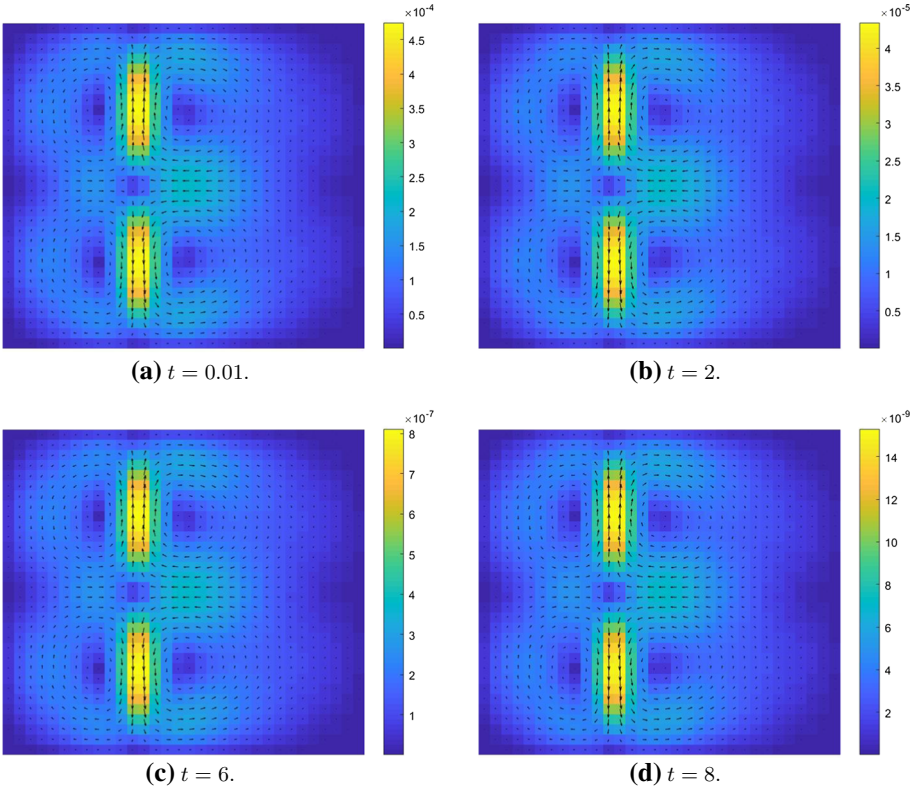

(a) $t = 0.01$. **(b)** $t = 2$. **(c)** $t = 6$. **(d)** $t = 8$.

Fig. 11 Snapshots of the velocity field at selected times with an initial temperature gradient perpendicular to the interface, where the interface is at $x = \frac{3}{8}$. **a v** at $t = 0.01$. **b v** at $t = 2$. **c v** at $t = 6$. **d v** at $t = 8$. From the velocity field at the interface depicted in (**b**–**d**), it shows that the velocity direction at $x = \frac{3}{8}$ is parallel to the interface, which is also verified by the distribution of the phase field in Fig. 10b. As the temperature gradient reduces, the velocity field also ceases

Table 1 Physical properties of acetonitrile and n-hexane

Property	Acetonitrile	*n*-Hexane
ρ (10^3 kg m^{-3})	0.776	0.655
ν (10^{-6} m^2 s^{-1})	0.476	0.458
D_0 (10^{-1} J m^{-1} s^{-1} K^{-1})	1.88	1.20
C (10^3 J kg^{-1} K^{-1})	2.23	2.27
σ (10^{-3} N m^{-1})	28.66	17.89

Remark 5.1 The above numerical experiments are simulated using the EQ Scheme. We repeat the simulations on thermocapillary convection case using the SVM scheme with the same parameter values and initial conditions. The results are essentially indistinguishable. Fig-

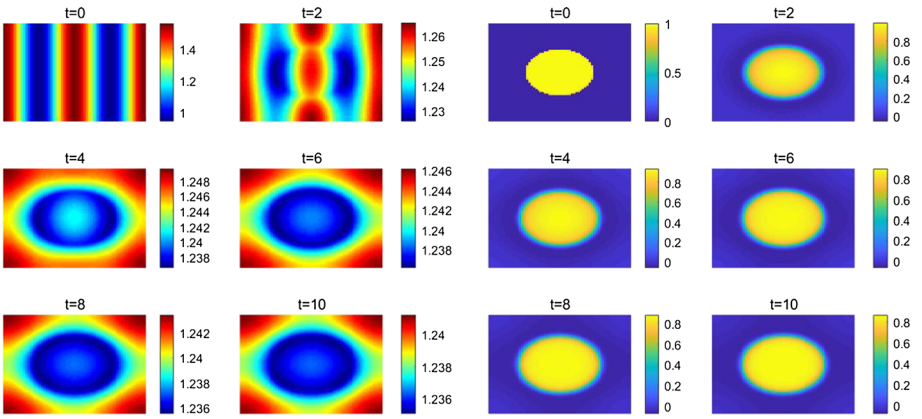

(a) Temperature field T. **(b)** Phase field ϕ.

Fig. 12 Snapshots of the temperature field and phase field at selected times. **a** The temperature field at $t = 0, 2, 4, 6, 8, 10$, respectively. **b** The phase field at $t = 0, 2, 4, 6, 8, 10$, respectively. At the onset of the simulation, some mixing is going on at the interface region due to transverse motion of the fluid flow so that the interface becomes fuzzy. As the gradient reduces, the interface motion ceases so that the interface becomes sharp again at the end of the simulation

ure 15a–c present the L^2 error between the solutions computed using the two schemes in $\phi, e, \sqrt{u^2 + v^2}$ over time, respectively. Both preserve the volume of each fluid phase, total energy and positive entropy production rate. The supplementary variable is consistently in the order of $O(\Delta t^2)$ shown in Fig. 15d. We note that we used Eq. (4.77) for computing $\alpha(t^{n+1/2})$ in the simulations using the SVM method.

6 Conclusion

In this article, we develop a new thermodynamically consistent, non-isothermal, incompressible, binary viscous fluid flow model and show that the model is dissipative with a positive entropy-production-rate when subject to appropriate boundary conditions. In order to devise a numerical scheme that preserves the thermodynamic consistency, the entropy quadratization method and the supplementary variable method are employed, which yields two semi-discrete numerical schemes in time and their fully discrete versions while the spatial discretization is carried out on the semi-discrete schemes using a finite difference method on staggered grids subsequently. Both schemes are second order, energy conserving, volume-preserving and entropy-production-rate preserving, in which one is weakly nonlinear while the other is linear and decoupled. The structure-preserving property and linearity of the second scheme is attained owing to the addition of the supplementary variable. We then carry out a series of mesh refinement tests to confirm the order of the schemes in both space and time. A couple of numerical examples are given to show the thermocapillary effect described by the hydrodynamic model in an immiscible binary viscous fluid system using the code implemented with one of the schemes.

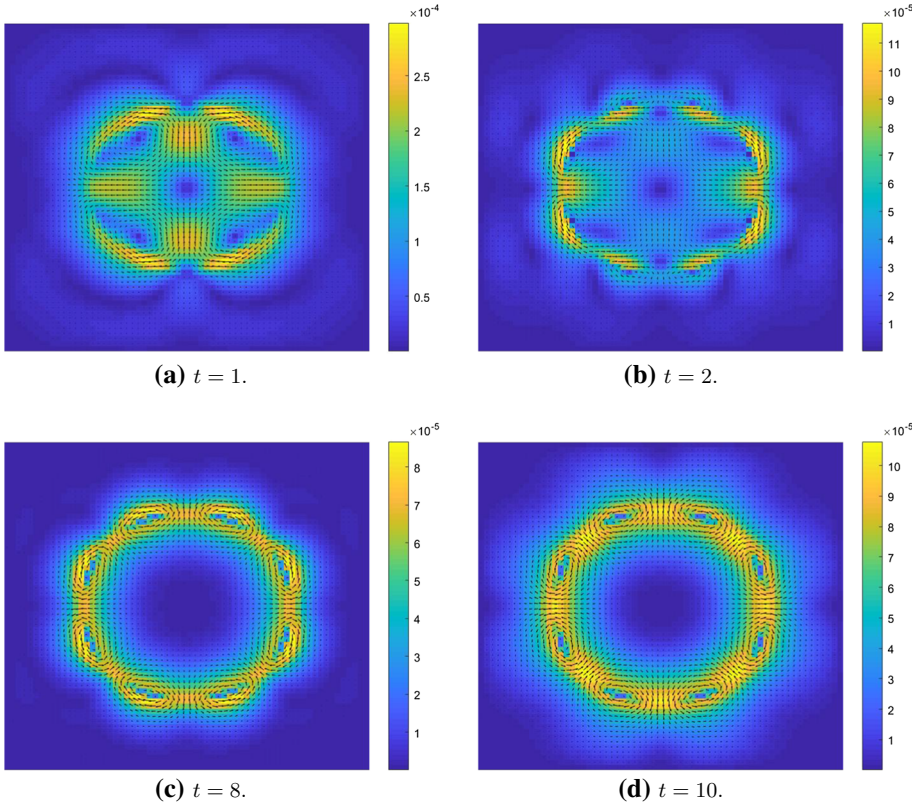

(a) $t = 1$. **(b)** $t = 2$.

(c) $t = 8$. **(d)** $t = 10$.

Fig. 13 Snapshots of velocity field at selected times. **a** **v** at $t = 1$. **b** **v** at $t = 2$. **c** **v** at $t = 8$. **d** **v** at $t = 10$. At the initial moment $t = 0$ and $t = 2$, there are different temperature gradients, the corresponding velocity fields are shown in (**a**, **b**), respectively. As the entropy increases in the dissipative system, the temperature gradient only remains at the interface while there is literally no temperature gradient in the bulk. Hence, the roll cells only survive at the interface instead of in the bulk as shown in (**c**, **d**)

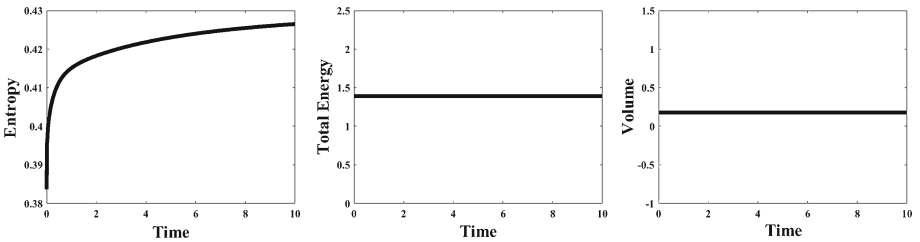

(a) Entropy S. **(b)** Total energy E. **(c)** Volume V.

Fig. 14 Evolution of the entropy, total energy and volume of the system over time. **a** The entropy S. **b** The total energy E. **c** The volume V. It demonstrates that the scheme preserves the thermodynamic consistency and volume

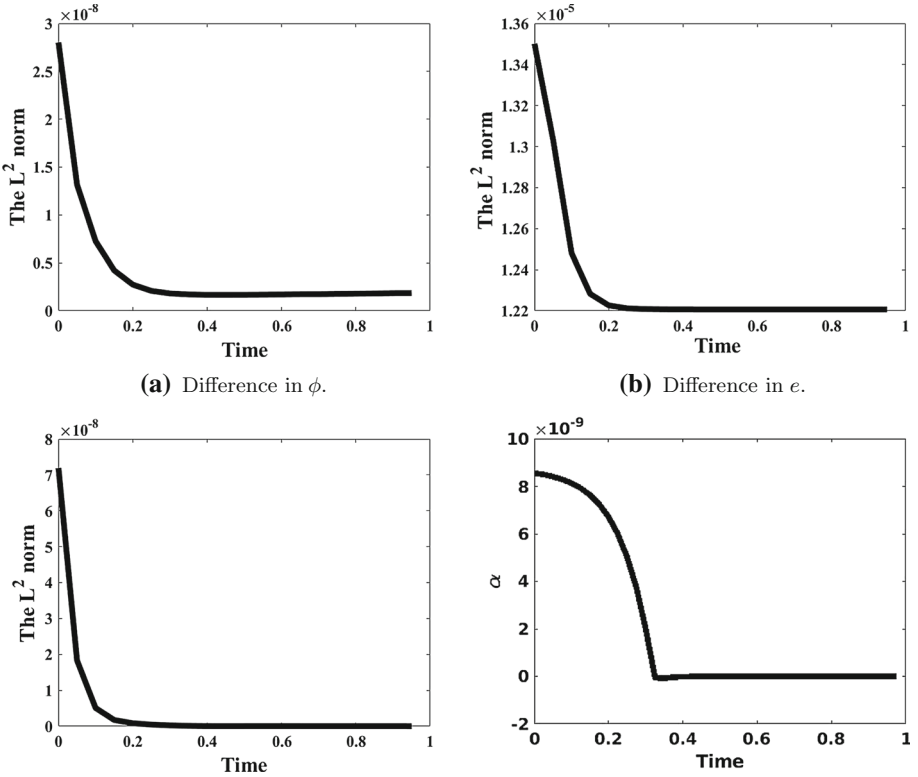

(a) Difference in ϕ. **(b)** Difference in e.

(c) Difference in velocity $\mathbf{v}$. **(d)** Supplementary variable α.

Fig. 15 Evolution of the difference in the L^2 norm in $\phi, e, \sqrt{u^2+v^2}$ between the solution computed using the two schemes over time. **a** Difference in ϕ: $\|\phi_{EQ} - \phi_{SVM}\|_2$. **b** Difference in e: $\|e_{EQ} - e_{SVM}\|_2$. **c** Difference in velocity $\mathbf{v}$: $\|\mathbf{v}_{EQ} - \mathbf{v}_{SVM}\|_2$. **d** The evolution of supplementary variable α. This indicates that α is consistently in the order of $O(\Delta t^2)$ in the simulation

Acknowledgements The research is partially supported by National Science Foundation DMS-1816783 award, DMS-1815921, OIA-1655740 and a GEAR award from SC EPSCoR/IDeA Program, NSFC awards #11801269 #11301287 and NSAF-U1930402.

References

1. Adamson, A.W., Gast, A.P.: Physical Chemistry of Surfaces, 3rd edn. Wiley, New York (1976)
2. Bestehorn, M.: Phase and amplitude instabilities for Benard–Marangoni convection in fluid layers with large aspect ratio. Phys. Rev. E **48**(5), 3622 (1993)
3. Bird, R.B., Armstrong, R.C., Hassager, O.: Dynamics of Polymeric Liquids, Volume 1: Fluid Mechanics, 2nd edn. Wiley, Hoboken (1978)
4. Boyer, F.: Mathematical study of multiphase flow under shear through order parameter formulation. Asymptot. Anal. **20**(2), 175–212 (1999)
5. Cahn, J.W., Hilliard, J.E.: Free energy of a non-uniform system. I. Interfacial free energy. J. Chem. Phys. **28**(2), 258–267 (1958)

6. Cheng, Q., Liu, C., Shen, J.: A new Lagrange multiplier approach for gradient flows. Comput. Methods Appl. Mech. Eng. **367**, 113070 (2020)
7. Du, Q., Liu, C., Wang, X.: A phase field approach in the numerical study of the elastic bending energy for vesicle membranes. J. Comput. Phys. **198**(2), 450–468 (2004)
8. Du, Q., Nicolaides, R.A.: Numerical analysis of a continuum model of phase transition. SIAM J. Numer. Anal. **28**(5), 1310–1322 (1991)
9. Francesco, D.A., Liu, C.: Non-isothermal general Ericksen–Leslie system: derivation, analysis and thermodynamic consistency. Arch. Ration. Mech. Anal. **231**(2), 637–717 (2019)
10. Gong, Y.Z., Liu, X.F., Wang, Q.: Fully discretized energy stable schemes for hydrodynamic equations governing two-phase viscous fluid flows. J. Sci. Comput. **69**(3), 1–25 (2016)
11. Gong, Y.Z., Zhao, J., Wang, Q.: Second order fully discrete energy stable methods on staggered grids for hydrodynamic phase field models of binary viscous fluids. SIAM J. Sci. Comput. **40**(2), B528–B553 (2018)
12. Guo, Z.L., Lin, P.: A thermodynamically consistent phase-field model for two-phase flows with thermocapillary effects. J. Fluid Mech. **766**, 226–271 (2015)
13. Guo, Z.L., Lin, P., Wang, Y.F.: Continuous finite element schemes for a phase field model in two-layer fluid Benard–Marangoni convection computations. Comput. Phys. Commun. **185**(1), 63–78 (2014)
14. Gurtin, M.E., Polignone, D., Vinals, J.: Two-phase binary fluids and immiscible fluids described by an order parameter. Math. Methods Appl. Sci. **6**(6), 815–831 (1996)
15. Helmut, A.: On a diffuse interface model for two-phase flows of viscous, incompressible fluids with matched densities. Arch. Ration. Mech. Anal. **194**(2), 463–506 (2009)
16. Juel, A., Burgess, J.M., McCormick, W.D., Swift, J.B., Swinney, H.L.: Surface tension-driven convection patterns in two liquid layers. Physica D **143**(1–4), 169–186 (2000)
17. Li, J., Zhao, J., Wang, Q.: Energy and entropy preserving numerical approximations of thermodynamically consistent crystal growth models. J. Comput. Phys. **328**, 202–220 (2019)
18. Liu, C., Shen, J.: A phase field model for the mixture of two incompressible fluids and its approximation by a Fourier-spectral method. Physica D Nonlinear Phenom. **179**(3), 211–228 (2003)
19. Liu, H.H., Valocchi, A.J., Zhang, Y.H., Kang, Q.J.: Phase-field-based lattice Boltzmann finite-difference model for simulating thermocapillary flows. Phys. Rev. E **87**(1), 013010-1–013010-13 (2013)
20. Liu, P., Wu, S., Liu, C.: Non-isothermal electrokinetics: energetic variational approach. Commun. Math. Sci. **16**(5), 1451–1463 (2017)
21. Liu, Q.S., Roux, B., Velarde, M.G.: Thermocapillary convection in two-layer systems. Int. J. Heat Mass Transf. **41**(11), 1499–1511 (1998)
22. Lowengrub, J., Truskinovsky, L.: Quasi-incompressible Cahn–Hilliard fluids and topological transitions. Proc. R. Soc. A Math. Phys. Eng. Sci. **454**(1978), 2617–2654 (1998)
23. Pendse, B., Esmaeeli, A.: An analytical solution for thermocapillary-driven convection of superimposed fluids at zero Reynolds and Marangoni numbers. Int. J. Therm. Sci. **49**(7), 1147–1155 (2010)
24. Shan, X.W.: Simulation of Rayleigh–Benard convection using a lattice Boltzmann method. Phys. Rev. E **55**(3), 2780–2788 (1997)
25. Tavener, S.J., Cliffe, K.A.: Two-fluid Marangoni Benard convection with a deformable interface. J. Comput. Phys. **182**(1), 277–300 (2002)
26. Teigen, K.E., Song, P., Lowengrub, J., Voigt, A.: A diffuse-interface method for two-phase flows with soluble surfactants. J. Comput. Phys. **230**(2), 375–393 (2011)
27. Velzen, D.V., Cardozo, R.L., Langenkamp, H.: A liquid viscosity–temperature–chemical constitution relation for organic compounds. Ind. Eng. Chem. Fundam. **11**(1), 20–25 (1972)
28. Yang, X., Li, J., Forest, M., Wang, Q.: Hydrodynamic theories for flows of active liquid crystals and the generalized onsager principle. Entropy **18**(6), 202 (2016)
29. Yang, X., Zhao, J., He, X.: Linear, second order and unconditionally energy stable schemes for the viscous Cahn–Hilliard equation with hyperbolic relaxation using the invariant energy quadratization method. J. Comput. Appl. Math. **343**, 80–97 (2018)
30. Yang, X., Zhao, J., Wang, Q.: Numerical approximations for the molecular beam epitaxial growth model based on the invariant energy quadratization method. J. Comput. Phys. **333**, 104–127 (2017)
31. Yang, X., Zhao, J., Wang, Q., Shen, J.: Numerical approximations for a three-component Cahn–Hilliard phase-field model based on the invariant energy quadratization method. Math. Methods Appl. Sci. **27**(11), 1993–2030 (2017)
32. Yue, P., Feng, J., Liu, C., Shen, J.: A diffuse-interface method for simulating two-phase flows of complex fluids. J. Fluid Mech. **515**, 293–317 (2004)
33. Zhao, J., Wang, Q., Yang, X.: Numerical approximations to a new phase field model for two phase flows of complex fluids. Comput. Methods Appl. Mech. Eng. **310**, 77–97 (2016)

34. Zhao, J., Wang, Q., Yang, X.: Numerical approximations for a phase field dendritic crystal growth model based on the invariant energy quadratization approach. Int. J. Numer. Meth. Eng. **110**(3), 279–300 (2017)
35. Zhou, B.H., Liu, Q.S., Tang, Z.M.: Rayleigh–Marangoni–Benard instability in two-layer fluid system. Acta. Mech. Sin. **24**(4), 366–373 (2004)